6. Physics and Mechanics of Rock Destruction

Methodological aspects of blast energy release kinetics control in mineral mining

N. Efremovtsev, A. Efremovtsev, S. Kvitko
ICEMR RAS, ANO NOIV, Innovation Center Summit-XX! OOO, Moscow, Russia

ABSTRACT: The paper addresses some aspects aimed at the perfection of test methods and procedures for commercial explosives and respective detonation systems. The authors present the results of the development and tests of new compositions of commercial explosives.

1 THE RESEARCH BACKGROUND AND CURRENT IMPORTANCE

Methods of rock blasting control, and analysis of operational and economic results of the variation of fragmentation intensity are analyzed in papers and monographs by K.N. Trubetskoy, V.V. Adushkin, S.D. Viktorov, L.I. Baron, G.P. Demidyuk. N.N. Kazakov, V.A. Belin, V.M. Zakalinsky, E.I. Efremov, N.S. Efremovtsev and some other researchers. For the improvement of the quality of rock fragmented by blast and minimization of the yield of substandard size materials (fine-size materials in the construction sector) the trend today is toward smaller diameter boreholes and transition to medium diameter 80-120 mm boreholes (close to critical). Application of conventional composite granulated explosives in such non-ideal conditions of detonation results in significant reduction of their actual force, higher yield of oversize material, lower performance of excavation and haulage machinery.

It is a well-known fact that with specific tasks of blasting the proper choice of explosives and charge design options is very important for the efficient fragmentation of rock with certain physical and mechanical characteristics. The efficient mining of valuable crystalline materials and development of mineral deposits containing various ores and construction materials requires the application of explosive charges differing in energy release kinetics. It is a multiple-path task, as detonation velocity and force control of limited-size explosive charges can be solved by various methods.

The integrated effect of rock properties on their blastability (fragmentation by blast) is described in detail by N.S. Efremovtsev in Kachkanar deposit case studies. Rocks are classified as five categories by rock mass blastability with due account for natural fracturing and weathering of the rock mass, and as classes by structural features (grain size) and mineralogical composition .

The field test analysis performed by the authors proves the feasibility of substantiation of such factors as dynamics, conditions, kinetics of energy release and transfer to the rock mass, and their practical application in the research activities. It is important to numerically evaluate in detail the effect of these factors on the efficiency of blasting of rocks with different physical and mechanical characteristics, as well as on the extent of blast harmfulness for the surrounding man-made entities, human beings and natural environment. Moreover, it is necessary to take into account the effect of energy release kinetics and the parameters of a controlled detonation system on the efficiency and extent of comprehensive exploitation of mineral resources, as well as performance and energy intensity of the subsequent mining processes.

For optimization of detonation systems it is important to perform a system multilevel analysis and control of the processes of blasting energy release:

- in a layer, where reactions go, and in the area of detonation high-temperature product emission;
- along a charge length in boreholes or blastholes;
- in a pattern of boreholes or blastholes within the boundaries of a block to be broken with due account for the optimal level of mineral losses and dilution.

An important part of the research is the formation of models of designed and tested commercial explosives as multiple micro- and nanodisperse energy-saturated systems and investigation of the effect of their parameters on the kinetics of blast energy release and transfer to the media to be broken and having different physical-mechanical characteristics.

Operational, economic, seismic and environmental factors of optimization of detonation system energy release kinetics control for efficient fragmentation of the rock mass and safety of blasting processes are described in detail by N.N. Efremovtsev and P.N. Efremovtsev in their papers mentioned in the References below. The authors point out the non-linear nature of the detonation velocity effect on the performance and economics of mining processes. The scientific rationale of the efficient energy release kinetic, velocity and patterns of charge detonation in rock blasting is a multi-factor optimization engineering and economic task requiring due account for the environmental effect of blasting and for the seismic effect of the blast action on specially protected areas.

Scientific approach to blast energy kinetics control for efficient mineral mining is based on the proposed categorization of methods of regulation of commercial explosives explosive characteristics and on the classification of methods of commercial blast control in an effort to regulate rock mass breaking .

An important part of the research is the perfection of the test concept and technology for low-sensitivity explosives and the formation of methods and procedures aimed at the optimization of detonation systems for blast specific tasks. Consideration must be given to numerical estimates of the blast effective work redistribution due to minimization of the harmful effect (seismic action and shock air wave).

To the fullest extent possible the aspects of low-sensitivity explosives test are described in the Collected Works issued by the Institute of Chemical Physics of the USSR Academy of Sciences, in which the results of studies performed by K.K. Shvedov, V.V. Lavrov, B.N. Kukib, A.N. Afanasenkov, V.A. Sosnin, et al.

An explosion occurring under the effect of stressing environment serves a criterion of sensitivity and a relative hazard of explosives.

As a rule, the following can be taken as a relative sensitivity criterion:

- the minimal initiating pulse, which is characterized by the minimal amplitude of the initiating shock wave;

- weight and size of a booster.

The traditional methodological approach has the following shortcomings:

- high test labor input;

- the necessity of setting off a charge of a substantial weight in composite coarse-dispersion commercial explosives tests;

- subjective estimation of the presence of explosives residue and inability of this method to numerically estimate the relative change of charge detonation completeness;

- the proposed methods and procedures do not contain the estimation of numerical values of blast efficiency increase, redistribution of blast harmful effect energy to useful forms for blast specific tasks.

For the assessment of the sensitivity of explosives to explosive pulse types used in practice the results of visual observation of the presence of explosives residue, a blasting cone in the ground or dent in a test plate serve the criteria of normal detonation of limited-length charges

As a rule, a fact of a normal detonation process is registered based on the analysis of the results of visual observation of the presence of explosives residue, a blasting cone in the ground, size of a dent, mark size on a test plate. The absence of explosives residue prevents from judging on the change of completeness of the velocity of detonation in modified compositions tests. The practice of utilized TNT block tests performed by the authors within the framework of the Parameter-C Program has shown that in the absence of explosive material residue the velocity of seismic impulse formed under the effect of explosion (directly proportional to the actual velocity of detonation) may differ by 50-120%. More precise numerical estimates of a seismic impulse can be obtained for explosions of charges horizontally placed on the ground.

In general, it is important to once more emphasize the idea that earlier proposed methods and procedures for commercial explosives tests do not contain the estimation of the possible redistribution of blast energy spent on unproductive and dangerous blast action to useful forms of blast action.

An important component of the assessment of hazard of one or another explosive is the identification of conditions, which provide the propagation of the explosion process in a manner, which is most efficient for a specific task.

2. CHARACTERISTICS OF THE PROPOSED METHODOLOGICAL APPROACH

The methodological approach proposed by the authors for commercial explosives tests is peculiar for the following:

1. The test objective is not only the assessment of safety and explosive characteristics of commercial explosives, but also the optimization of detonation system parameters for specific tasks in specified mining conditions.

2. A multiple nano- and mictosystem model of a test commercial explosive composition is formed. Various methods of the regulation of explosive characteristics of commercial explosives are considered. Regulation methods (ECRM) are ranked by their importance for the task of explosives properties control. For the selected ECRM the possible and reasonable limits of energy-saturated material nano- and microdisperse system characteristics control are set. Variation of energy release kinetics of test charge designs is studied in detail for various methods of energy release kinetics control. Feasibility is also studied of the application of the wave method of explosives components modification.

3. In the course of detonation system optimization for charges of a desired length to decrease labor intensity of the pretest procedures use is made of the proposed contributing factor analytical dependences of explosive characteristics

4. Detonation velocity in steel tubes is estimated by a fiber-optic method. In open-type charges, pilot boreholes and blastholes the variation of the detonation front propagation velocity is measured continuously by a SpeedVOD instrument along the whole length of charges

5. For the assessment of the comparative force in addition to blasting-cone volume measurement the velocity of ground seismic vibrations and characteristics of a shock air wave, height and radius of flyrock travel are measured in comparable conditions. Color and other characteristics of detonation products are recorded.

6. On the basis of system analysis of the information on the variation of the force of test explosives and detonation systems on their basis the trends and numerical values of parameters characterizing the blast energy redistribution in useful and hazardous blast action forms are estimated.

7. The proposed methods and procedures are used for the assessment of the energy release kinetics effect of a test explosive or its detonation system on the fragmentation of rocks differing in brittleness and strength, and valuable crystalline materials.

The available instrumentation allows more precise and objective judgment on the relative variation of completeness and kinetics of explosive transformation. Moreover, the methods and procedures proposed by the authors for field tests require some changes in the pattern of charges and instrumentation location on the test site.

The experimental efforts of the authors are aimed at the perfection (structural modification at the nano- and micro-level) of the available compositions of commercial explosives and

development of new compositions, as well as the upgrading of charge design and improvement of the parameters of blasting processes to provide the most efficient solution for specific tasks of mining and construction:

- lower shattering effect of a blast to provide the undamaged condition of valuable crystalline materials and lower yield of fines in construction material mining;

- lower seismic effect of blast and shock air wave;

- higher intensity of fragmentation and radius of controlled rock fragmentation in ore deposit mining. (15)

Figure 1 shows the proposed layout of a test site, which is peculiar for the fact that charges are placed in a ring pattern at an equal distance from a seismographer rather than in straight lines. For the assessment of the sensitivity of commercial explosives and completeness of their detonation the test open-type charges in paper and plastic envelopes are placed horizontally rather than vertically on the ground with vegetable soil removed.

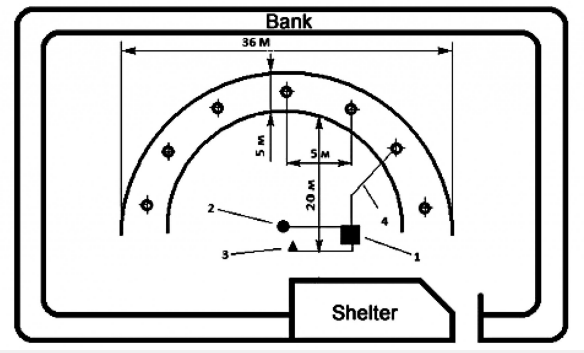

Figure 1. Field test site layout
1 – armored case for a seismographer and detonation velocity measuring instruments; 2 – microphone for measurement of shock air wave characteristics variation; 3 – seismic pickup; 4 – armored hollow shelter for optical fiber and cable; O – charge location point.

The proposed design of charges in cardboard envelopes for commercial explosives sensitivity tests and the assessment of transient detonation zone size variation is shown in Figure 2. Charges are placed horizontally on the ground and fired in turn. It makes possible the assessment of the comparative force judging by blasting-cone, seismic and acoustic components of test detonation system action in comparable conditions.

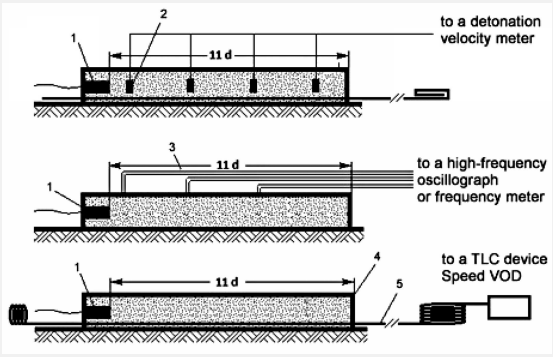

Figure 2. Charge design for horizontal placing to assess sensitivity to the initiating pulse, detonation velocity, variation of blast seismic action and shock air wave effect.
a, b, c – design of charges in steel tubes for contact method of detonation velocity assessment (closing sensors for detonation front passage), fiber-optic method of detonation velocity measurement, and TLCSheedVOD instrument.

1 – primer consisting of electric detonator and detonation block; 2 – steel tube envelope; 3 – optic fiber, 4 – detonation velocity measurement cable for TLCSheedVOD

Application of the methodological approach and instrumentation proposed by the authors provides a significant volume of additional information on a hazard level and efficiency of new commercial explosives with various detonation systems and allows standardization of the commercial explosives test methods and procedures.

For the enhancement of blast efficiency, expansion of the range and capabilities of explosive characteristics controllability of cheap commercial explosives, as well as safety of their application the ANO National Organization of Explosives Engineers has performed laboratory research and field tests. The results of these tests have served a basis for the development of new compositions of Granulites (Granulite EF-P, Specs. TU 7276-002-94120064-2009, and Granulite EF-PN, Specs. TU 7276-003-94120064-2009), and elaboration of some aspects of the fabrication technology on use sites and borehole-charging areas.

3. METHODOLOGICAL ASPECTS OF LABORATORY AND FIELD TESTS

Laboratory tests of new explosives compositions formed an important methodological part of the research. The laboratory tests pursued the following main objectives:

- changing the retention capacity of granules of porous and smooth ammonium nitrate with the use of a various emulsifier compositions and conditions of their exposure to physical fields;

- effect of the composition of various emulsifiers on the emulsion stability and retention capacity;

- effect of ultrasonic exposure and magnetic pulse treatment in fields of complicated spatiotemporal structure with

the use of a GAN 5000 plant on the kinetics of ammonium nitrate decomposition and energy release in conditions of combustion and detonation, and on the absorption capacity of an oxidizer;

- fuel emulsion dispersion and stability;

- assessment of the Granulite EF sensitivity to impact according to the GOST 4545-88 standard and with a K-44-3 instrument;

- research into the kinetics of energy release of composite commercial explosives and their components.

The laboratory tests were performed in cooperation with experts from the Institute of Chemical Physics, RAS, the National Research Nuclear University MEPhI and the The Federal Center for Dual-Use Technologies Soyuz.

The research into the kinetics of thermal decomposition was carries out in MEPhI with a NETZSCHSTA 409 instrument, as well as in the ICEMR RAS with the use of a Q-15000 thermogravimetric analyzer. The results were analyzed with Ecochrom software. The effect of Granulite exposure to physical fields and concentration of various energy additives on energy release kinetics was investigated in every detail.

Dynamics of the detonation front, kinetics of the processes of detonation transition to accelerated combustion, and characteristics of high-temperature gas detonation products (blasting medium), indices of blast seismic action and shock air wave were studied in the process of field tests in steel tubes with the use of fiber-optic method.

The effect of detonation velocity, charge design and layout, physical properties of rocks is investigated in the process of field tests with the used of methods and procedures proposed by the authors and envisaging the application of simulation models of blast media and rock samples differing in brittleness and uniaxial compression strength. The proposed methods and procedures include the assessment of energy release kinetics of special-design charges located at different distances from test samples of rocks having different physical properties in terms of crushability and residual strength.

Dispersion and through-time stability of fuel emulsion compositions used for the fabrication of Granulite EF compositions designed by the authors were studied with the use of a D-1200 electroacoustic spectrometer. Research into the microstructure of ammonium nitrate was carried out with the use of HITACHITM-1000 scanning electron microscope. The results of dispersion emulsion microstructure studies are shown in Figure 3. Photographs of the surface of smooth ammonium nitrate before and after treatment are shown in Figure 4 and Figure 5.

4. SUMMARY AND CONCLUSIONS

1. The new cheap commercial explosive composition differs from ANFO or Igdanite in the application of a complex oil-in-water emulsion instead of diesel fuel. This water-based emulsion is a nano-microdispersion mixture of mineral oil, diesel fuel and emulsifiers-catalysts providing a more accelerated and complete process of chemical reactions.

2. Investigation of the surface of ammonium nitrate with a HITACHITM-1000 scanning electron microscope has shown that the contact of the proposed fuel mixture with the surface of ammonium nitrate granules gives rise to the formation of pores in the latter, and the fuel mixture evenly fills the framework structure of the oxidizer thus providing multiple expansion of the fuel and oxidizer contact area, with a granule shape being unchanged. The emulsion globule size is by several orders of magnitude less than that of ammonium nitrate pores, and therefore it easily penetrates deep into ammonium nitrate granules (see Figure 5). Fuel and catalysts of primary and secondary reactions, sensitizing agents and energy additives penetrate into ammonium nitrate granules, and they are evenly distributed in granule volume, thus by several orders of magnitude expanding the area of the fuel and oxidizer contact.

3. Investigation of Granulite EF fuel component dispersion with the use of D-1200 electroacoustic spectrometer has shown that the globule size of the micro-nano-dispersion emulsion proposed by the authors is 2.4 microns and 450 nanometers (see Figure 3). The emulsion is characterized by high stability and rather narrow range of globule size variation.

4. The advantage of new compositions of commercial explosives and detonation systems on their basis, explosives fabrication and borehole charging technologies with the use of mix-pump trucks is in the fact that it is possible to promptly change the proportions of the emulsion components, their concentration in the end mixture, and accordingly, their explosive characteristics and explosives energy release kinetics along the length of bore- or blastholes, to enhance energy-saturated systems of some parts of a detonation system and charges in the process of formation of their bases and main sections, to control pressure and its kinetics, parameters of load distribution and blast energy transfer to the rock mass, and accordingly, the radius of its controlled fragmentation, as well as particle-size distribution of rock broken by blast.

5. The proposed new commercial explosives and detonation systems on their basis underwent field tests in 2007 – 2011 and proved an opportunity of 130% enhancement of the charge efficiency in terms of blasting cone, with levels of blast and shock air wave dangerous seismic effect actually being unchanged. The highest efficiency was demonstrated by detonation systems of combined Granulite EF-P and Granulite EF-PN charges.

6. In experiment it was found that by way of in-process correction of the emulsion composition it was possible to decrease the flyrock travel by 50-70% with high quality of the broken material being kept. The test results are validated by the joint test certificate of OOO Vzryvstroy and ANO National Organization of Explosives Engineers.

7. A program of mix-pump truck modernization is available for the expansion of the functional capabilities and in-process control of energy saturation and environmental safety of the application of detonation systems with an expanded range of their explosive characteristics control.

8. The results of laboratory tests of Granulite new compositions performed by FGUP Federal Center for Dual-Use

Technologies Soyuz (federal state unitary enterprise) are shown in the Table 1.

Explosive	Sensitivity to impact: weight: 10 kg, lower limit, mm	Impact minimal energy, J	Sensitivity to friction, Po, kgf/cm^2	Temperature of initial intensive decomposition, ^{0}C	Flashpoint, ^{0}C
Granulite EF-P	500-0	49.1	6,780	231	250
Granulite EF-PN	500-0	49.1	6,780	256	260

Table 1. Results of laboratory tests of Granulite new compositions

9. Thus, the proposed commercial explosives and technologies of the formation of a framework nano- and microdisperse structures of explosive material components and detonation systems on their basis allow to significantly broaden the opportunities of in-process control of explosive characteristics, formation of charges with variable energy saturation and kinetics of blast energy release and transfer to the rock mass to enhance the efficiency of detonation system charges with no losses in safety of their application.

9. On the basis of Granulite EF and Granulite EF-P formulas new compositions are developed of commercial powder-like and water-resistant emulsion explosives with enhanced energy saturation, as well as compositions of explosives for low-impact blasting. An important advantage of explosives new compositions is an opportunity of their application in small-diameter boreholes and blastholes, adjustment of explosive characteristics of detonation systems within a broad range depending on blast specific tasks and mining conditions.

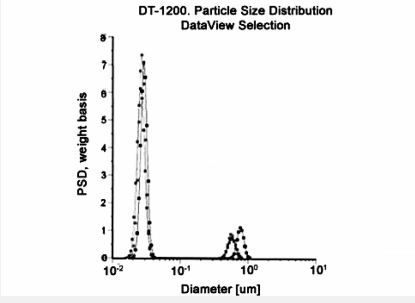

Figure 3. Results of Granulite EFs fuel emulsion nano- and microstructure studies with the use of D-1200 electroacoustic spectrometer.

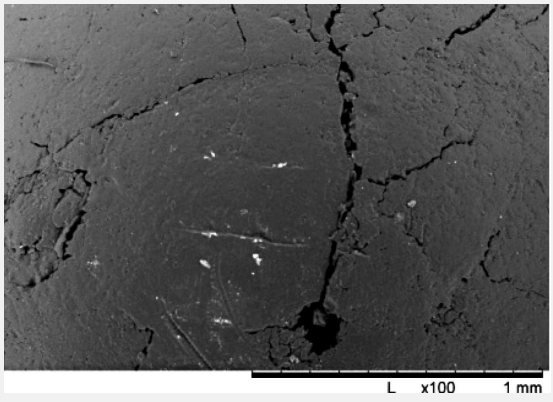

Figure 4. Photograph of the surface of ammonium nitrate, grade A, GOST 2-85 standard, taken with the use of a HITACHITM-1000 microscope.

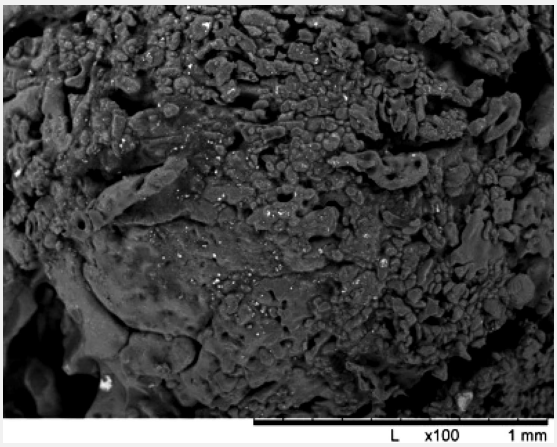

Figure 5. Photograph of the surface of ammonium nitrate, grade A, GOST 2-85 standard, taken after treatment with pore-forming emulsion in the process of Granulite EF-P and Granulite EF-PN fabrication. The image is taken with the use a HITACHITM-1000 microscope.

REFERENCES

Borovikov V.A., Andreev A.A. Efremovtsev N.N. 2007. Characteristics of detonation of Granulites including low-density polystyrene-containing compositions. *Gorny Informatsionno-Analitichesky Bulletin. Vzryvnoye Delo. Collected works. MSMU Publishers.* (in Russian)

Efremov E.I., Nikiforova V.A. et al. 2001. On the interrelation of fines yield in rock blasting and pulse parameters of various explosives. *Metallurgicheskaya I Gornaya Promyshlennost,* No 1: 88-90. (in Russian)

Efremovtsev N.N. 2012. Chatacteristics of the formation of multiple micro- and nanodisperse systems of Granulites EF and commercial water-resistant emulsion explosives on their basis. *Collected works: Voprosy nauchnogo obosnovsaniya sovershenstvovaniya sredstv upravleniya intensivnostyu razrusheniya gornykh porod vzryvom.No 12. Special Issue:* 17-24. (in Russian)

Efremovtsev N.N. Classification of methods of explosive characteristics control for commercial explosives. 2007. *Gorny Informatsionno-Analitichesky Bulletin. Vzryvnoye Delo Collected works. Vol. 2, MSMU Publishers.* (in Russian)

Efremovtsev N.N. Engineering and economic factors of optimization of detonation system energy release kinetics control for reasonable fragmentation of rocks by blast. 2012. Collected works: *Voprosy nauchnogo obosnovsaniya sovershenstvovaniya sredstv upravleniya intensivnostyu razrusheniya gornykh porod vzryvom.No 12. Special Issue:* 3-10 (in Russian)

Efremovtsev N.N., Efremovtsev P.N. 2012. Seismic and environmental factors of the optimization of detonation system energy release kinetics control for safety of blasting processes. *Collected works: Voprosy nauchnogo obosnovsaniya sovershenstvovaniya sredstv upravleniya intensivnostyu*

razrusheniya gornykh porod vzryvom. No 12. Special Issue: 11-16. (in Russian)

Efremovtsev N.N., Kazakov N.N. 2012. Revisited: Formation of the classification of control methods of energy release kinetics and transfer to the rock mass for its breakage with a desired degree of fragmentation. 2012, *Collected works: Voprosy nauchnogo obosnovsaniya sovershenstvovaniya sredstv upravleniya intensivnostyu razrusheniya gornykh porod vzryvom. No 12. Special Issue:* 27-32 (in Russian)

Efremovtsev N.N., Kvitko S.I., Pozdnyakov A.S. 2012. About the program of mix-pump truck modernization for the expansion of the functional capabilities of blast action control. *Collected works: Voprosy nauchnogo obosnovsaniya sovershenstvovaniya sredstv upravleniya intensivnostyu razrusheniya gornykh porod vzryvom.No 12. Special Issue:* 23-26. (in Russian)

Efremovtsev N.N., Sosnin A.V, Belin V.A., Efremovtsev A.N. 2008. Development of simulation models for charge blast assessment in terms of valuable crystalline materials undamaged condition. *Vzryvnoye Delo Collected works. No 157* (in Russian).

Efremovtsev N.S. 1968. Investigation and on-the-job assessment of properties of rock as blast media in conditions of mineral deposit surface mining: Kachkanar GOK Case Study. 1968. *Author's abstract of a thesis.* Magnitogorsk: 43. (in Russian)

Intensification of rock blasting for continuous operation machinery. 1967. *Vzryvnoe Delo,* No 62/19: 316 (in Russian)

Methods of low-sensitivity explosives tests. Best Practices. Under editorship of Shvedov K.K. 1991. Institute of Chemical Physics, USSR Academy of Sciences, Chernogolovka: 149. (in Russian)

Trubetskoy K.N., Melgunov V.G. 1975. The effect of lump size of rock on the performance and economics of loaders. 1975. *Gorny Zhurnal,* No 11: 22-24 (in Russian)

Trubetskoy K.N., Viktorov S.D., Kutuzov B.N. 2009. Problems of blasting processes evolution on the ground surface. *Vzryvnoe Delo,* No 101/58: 3-33. (in Russian)

Viktorov S.D., Kazakov N.N., Zakalinsky V.A. 1995. Analysis of methods of rock blasting process control. *Gorny Zhurnal* No 7: 46-47 (in Russian).

Assessment of the transmissibility of blasting vibrations from rock to seismographs

P. Segarra, J.A. Sanchidrián, L.M. López, R. Castedo
Universidad Politécnica de Madrid – E.T.S.I. Minas. Rios Rosas, 21. 28003 Madrid, Spain.

I. del Castillo
VIBRAQUIPO. Gaiteiro de Soutelo, 3. 36004 Pontevedra, Spain.

ABSTRACT: This work investigates the performance of some of the measurement techniques used in vibrations from blasting monitoring. Two tri-axial geophones with cases of different size, shape and mass were tested in the laboratory. The geophone cases were mounted in three different ways on a granite slab fixed to a shaker table: freely placed, sandbagged, and anchored. A known horizontal periodic motion of constant amplitude and frequency from 16 to 200 Hz was applied to the slab. Two amplitude levels of 5 and 20 mm/s were applied when the sensors were sandbagged or anchored and only 5 mm/s when no holding force was applied. The transmissibility of vibrations from the slab to the longitudinal geophone as function of the frequency (i.e. ratio of response of the geophone to the slab motion) has been obtained for each measuring condition tested. Such values are an estimate of the overall error for the horizontal components (either longitudinal or transversal) in vibration records. From them and the baseline error determined with the sensor directly anchored to the shaker, the measurement error was obtained. Sensor freely placed on the rock does not provide a good contact with the ground and results depend on the weight of the sensor case. Ground motion is amplified by a factor of 1.12 of the rock motion (i.e. a gain around 1.0 dB) at 52.1 Hz for the heavier sensor's case and at 71.3 Hz for the lighter; they provide, however, negligible errors at frequencies less than 28 and 40 Hz, respectively. For frequencies above the resonant, the ground motion in the horizontal component is strongly damped by the sensor. Anchored sensors monotonically amplify the input velocity in the frequency range considered, but at a lower rate; a transmissibility up to 1.02 (0.17 dB) is obtained in the common frequency range for blasting (frequencies below 100 Hz). Sandbagging encompasses low reproducibility of the sensor response due to variations in the bag positioning, inherent to this fixation method, and also bad performance if the contact surface is small. The slab motion is damped in the sensor response to 0.78 (-2.16 dB) at low and mid frequencies, and is amplified between 1.07 and 1.2 (0.59 and 1.58 dB, respectively) depending on the test, at high frequencies. Errors are also analyzed as function of the input acceleration levels suggested by common field guidelines. Results encourage considering other factors to decide the coupling method.

1. INTRODUCTION

Ground vibrations from blasting are often the main source of complaints and litigations to mines and quarries in populated areas. Measurement of ground motion is necessary to assess compliance with national standards (Siskind et al. 1980, AENOR 1993, BSI 1993, DIN 1999, Singh & Roy 2010) and prevent damage to buildings and structures. The conclusions from vibration control studies depend on how well the measured magnitudes represent the actual seismic field. A first source of error is due to the amplitude response of the seismograph, i.e. geophone and recording unit. The measurement techniques, mainly sensors mounting, are another source of error. The coupling method is often selected as function of the expected acceleration and the ground type, rock or soil, at the monitoring point (ISRM 1992, ISEE 2009) to prevent that the sensor loses contact in the vertical or slides in the horizontal direction. The distortion of the response characteristics due to the coupling conditions of the sensor with the ground (Washburn & Wiley 1941, Hoover & O'Brien 1980, Khron 1984, Blair 1995a; Drijkoningen et al. 2006) is often disregarded.

Research in this area is constrained by the fact that the actual seismic field from blasting is unknown and unique. This limitation is solved by placing several sensors right next to one another in the field, so that a set of samples of the actual seismic field is obtained. Some studies used different mounting method in each blast to assess the relative performance of the methods tested (Blair 1995b, Armstrong & Sen 1999, Williams & Treleaven 2003, Adhikari et al. 2005, Hutchison et al. 2005, Wheeler 2004). Other works estimate the uncertainties or dispersion in vibration measurements from data obtained with the sensors coupled in the same way (Armstrong 2001, Segarra et al. 2010, 2012a, 2012b). Another approach to the coupling problem consists of transmitting a known vibration motion, usually a periodic wave, to the media in which the sensor case is mounted, and analyzing the geophone response. Shaker tables with the transducer coupled directly to the table or to the soil loaded into a box attached to the table allow this type of testing (Krohn 1984, Blair 1987, 1995a, Farnfield 1996). In these experiments, no scattering response is produced as no travelling waves are induced by the shaker movement. This, however, is not a problem when the transmissibility of vibrations from rock to sensor is analyzed; in this case the total response is equal to the radiation response, as the scattering response is negligible. Other techniques are used to assess sensor coupling to soil (Washburn & Wiley 1941, Hoover & O'Brien 1980, Drijkoningen 2000).

This study gives an insight to the quality of vibration measurements (i.e. accuracy and reproducibility) from blasting in horizontal directions. A shaker table has been used to obtain the transmissibility of vibrations as function of the frequency for two seismographs coupled to the rock with three methods (12 tests).

2. EXPERIMENTS AND INSTRUMENTATION

The experimental work was made with a computer controlled shaker capable of a force of 144 kN at VIBRAEQUIPO facilities (Pontevedra, Spain). The shaker table was arranged to vibrate horizontally. Tests in the vertical direction were discarded to

prevent damage to the shaker. The shaker table flow sheet is shown in Figure 1 and it is summarized next. A drive signal is supplied via a power amplifier to the shaker. This induces to the table a vibratory movement which velocity is measured with a resolution less than 0.003 mm/s at 200 Hz by a laser Doppler vibrometer (LDV). The LDV output is fed back to the vibration controller to correct the drive signal in real time. The drive signal amplitude was kept constant within an error up to 1 % of the nominal value, and its frequency was shifted with an error less than 0.01 % from 16 to 200 Hz at a rate of 0.02 octaves/s through a power law sweep. The frequency range is a compromise between the memory capacity of the recording units on one side, and both the predominant frequencies of vibrations from blasting, and the frequencies of resonance of the coupling methods on the other. It should be noticed that some of the resonant frequencies of typical urban dwellings (Siskind et al. 1980) are outside the range considered here.

Table 1 shows the characteristics of the two seismographs used. They are identified as Y and Z to avoid any manufacturer or commercial reference. These devices are formed by three orthogonally oriented geophones housed in a metallic case and connected to a recording-sampling unit. A sampling rate of 2048 Hz, faster than the minimum rate suggested by ISEE guidelines (2009) was used. Table 2 shows the characteristics of the tests chronologically sorted. For each test type, seismograph Y was analyzed first and Z next. The longitudinal geophone was aligned with the direction of the movement of the shaker.

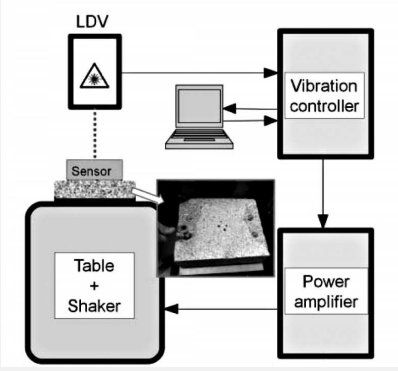

Figure 1. Shaker table

Table 1. Characteristics of vibration monitoring devices

Characteristics	Y	Z
Mount		
Density (kg/m^3)	2130	2690
Mass (kg)	0.905	0.508
Shape	Cylindrical	Prism
Size-radius[a]/height (mm/mm)	50/50	37/44
Anchor hole-radius (mm)	4.75	3
Geophone		
Frequency range (Hz)	2-250	2-250
Admissible accuracy from 4-125 Hz[b] (dB)	±0.5	±0.5
Recording-sampling unit		
Analog to digital converter (bits)	12	16
Range/Resolution[c] (mm/s)	±254/0.127 ±31.7/0.0159	±200/0.006

[a] Equivalent radius of a circle with the same area than the contact surface.
[b] ISEE (2011).
[c] Seismograph Y allows two measuring ranges, each with a different resolution.

Tests identified as B0 aim to obtain the amplitude response or error of each seismograph. They were made according to the calibration procedure normally used in the laboratory, which consists of anchoring the sensors directly to the table and inducing a vibration motion of 10 mm/s. In the rest of the tests, the sensors were placed on the rough side of a grey granite slab of size 24.5 x 30 x 8 cm. The granite had a density of 2650 kg/m3, and an estimated p-wave velocity of 4425 m/s (Vázquez et al. 2010). The slab was fixed to the plate with four hex lag bolts (8 mm diameter) that were tightened to a torque of 4 N•m. The slab vibrates at 5 and 20 mm/s (half and twice the velocity used in B0, respectively) when the sensors were sandbagged or anchored and only at 5 mm/s when no holding force was applied to them. Higher input velocities were not used because they produce spurious amplitudes of around four times the input velocity that mask the result of the test (Faber & Maxwell 1997, explain this phenomena that does not take place when the sensors are subjected to non-periodic motion as occurs in blasting).

Figure 2 shows the layout for sensor cases held with a bag. Initially the bag had 5 kg of cat sand and a size of 23 x 32 x11 cm. Though larger bags are used in the field, these tests are useful to understand the effect of the sandbag in the transmissibility of vibrations. After testing both sensors with the sandbag at low velocities (SbL tests), the bag was deteriorated. This leads to a different bag profile and a greater contact between bag and rock in tests at high velocity (SbH), compare photographs (a-b) in Figure 2 with photographs (c-d).

Test acronym	No. tests	Placement	Coupling conditions	Input amplitude[b] (mm/s)
B_0	2	Table	Hex lag screws & washer[a]	10
FrL	2	Grey granite	No holding force (free)	5
SbL	2	Grey granite	Sandbag	5
SbH	2	Grey granite	Sandbag (deteriorated)	20
AL	2	Grey granite	Anchor, rod, washers & nut	5
AH	2	Grey granite	Anchor, rod, washers & nut	20

[a] A torque of 4 N·m was supplied to 8 and 6 mm diameter bolts for Y and Z, respectively.
[b] The resolution of seismograph Y was fixed at 0.127 mm/s for inputs of 20 mm/s, and at 0.0159 mm/s for other.

Table 2. Summary of the tests

Sensor anchoring was made by a plastic anchor (8 mm diameter and 40 mm long), a threaded rod (6 mm diameter), two washers and a nut. There was a tolerance between the case hole of geophone Y and the setting rod (see the anchor hole radius in Table 1); torque could not be controlled in this case.

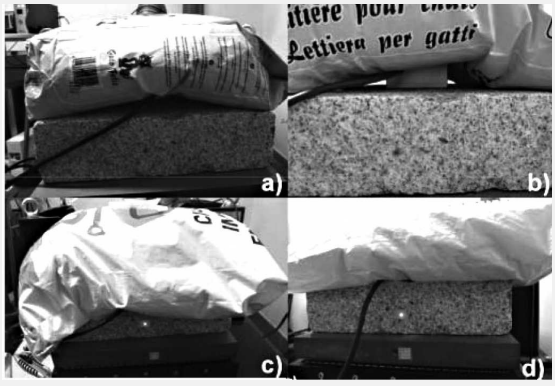

Figure 2. Layout of geophones held with sandbags at low-SbL (graphs a-b) and high velocities-SbH (graphs c-d).

3. RESULTS AND DISCUSSION

3.1 Data processing

All the analysis is based on the output from the longitudinal geophones. It is assumed that similar results will be obtained in other directions of the horizontal plane, such as the transversal, according to Segarra et al. (2012a) that could not observe statistical differences in the experimental error or uncertainties in the longitudinal and transversal components. The transmissibility of vibrations from the rock to the geophone is first explored qualitatively from the square root of the spectrograms. They are obtained by dividing the signals into segments and computing the short-time Fourier transform of each segment. The results are shown in the form of contours of the amplitude spectral density as function of time and frequency. Figure 3 shows them for tests in which seismograph Z was freely placed at low velocities (FrL), sandbagged at low and high velocities (SbL and SbH, respectively) and anchored at high velocities (AH); light contours correspond to high spectral densities, and dark to low values. The fundamental and other harmonics are marked as F and H, respectively. Similar results have been obtained from tests with sensor Y. In all the signals, the main energy trace corresponds to the power-law function of frequency versus time, from 16 to 200 Hz in about 182 s. For methods other than anchoring, the energy pattern is distorted and the sensor vibrates at other (higher) frequency modes; see the harmonics when the bag it is used, graphs (b) and mainly (c), which are likely produced by the sand vibration or by bag movement before reaching its steady state. Besides, there are monochromatic vibration modes independent of the excitation clearly apparent with free sensors; see the horizontal contours marked as M in graph (a).

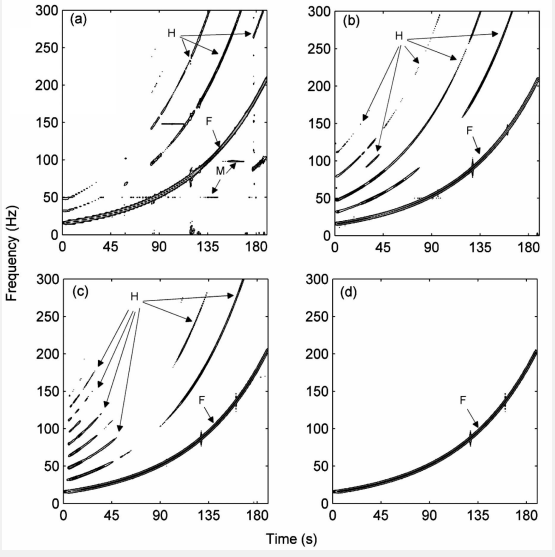

Figure 3.Modified spectrograms for seismograph Z: freely placed at low velocities, FrL (a), sandbagged at low velocities, SbL (b), sandbagged at high velocities, SbH (c), and anchored at high velocities, AH (d); F is the fundamental sweep, H are other harmonics, and M are monochromatic vibration modes.

The transmissibility of vibrations from the rock to the geophone (T) is expressed as function of the frequency and it is obtained from the ratio between the spectral densities of the geophone record (output) and those of the input, i.e. periodic motion of the material in contact with the sensor case or vibration in the absence of the sensor (Washburn & Wiley 1941, Drijkoningen et al. 2006). T can be understood as a quantitative statement of the total error committed in the tests, and is also given as a gain G=20•log (T). Non-processed or raw transmissibility has a large variance or noise, as can be seen in Figure 4. It shows the transmissibility of the seismographs from test B0. In order to filter out that noise, the following method is used: i) Bartlett's method is applied to calculate the amplitude spectral density; ii) T is calculated; and iii) a further smoothing is made trough a robust locally weighted linear regression with linear polynomials (robust lowess method, Cleveland 1979). Figure 4 shows that good results are obtained, when 8 segments are used to estimate the spectral density and a span of 8 % is considered for the robust regression.

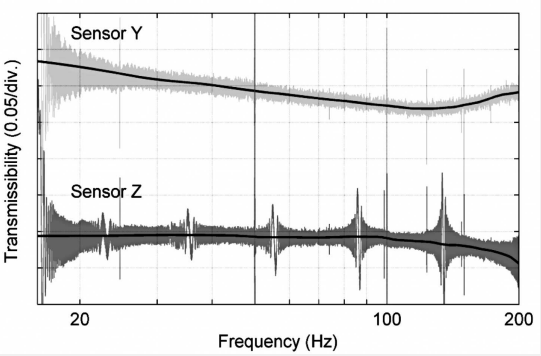

Figure 4. Transmissibility of the seismographs obtained in test B0 (grey lines are raw values; dark thick lines are smoothed values).

To obtain the transmissibility of vibrations due to coupling conditions, TC (i.e. measuring error), the total transmissibility, TT, is divided by the transmissibility of the seismographs, TS. The coupling transmissibility-TC curves- obtained in the tests in which the coupling conditions were implemented are plotted in Figure 5. Because the transmissibility of the geophones varies in a tight range 0.96 to 1.03 (-0.35 to 0.26 dB), TT is similar to TC and the former is not plotted here for the sake of simplicity.

3.2 Transmissibility of anchored sensors

If the sensors are anchored, the slab motion is amplified only up to 1.02 (0.17 dB) in the common frequency range for blasting (frequencies below 100 Hz); the coupling resonance is above 200 Hz. The dispersion is low with a maximum difference between transmissibility curves from anchored geophones less than 0.02.

3.3 Transmissibility of free sensors

Sensors freely placed on the rock follow acceptably well the slab motion (i.e. transmissibility from 0.98 to 1.02) in a narrow range of frequencies: 16-28 Hz for Y and 16-40 Hz for Z. The amplitude of the resonance peak is around 1.12 (0.98 dB) and occurs at 52.1 Hz for sensor Y, and 71.3 Hz for Z. Above the resonance frequency, rock motion is strongly damped in the sensor. This is the worst scenario, when compliance is assessed. Interestingly

vertical velocity increases more than one order of magnitude for frequencies higher than the resonant. Published works (Hoover & O'brien 1980; Blair 1995a) show that differences in the amplitude response can be explained using the planting factor P that it is defined here as the ratio between the mass of the geophone and the product of the rock density to the geophone case volume. These works show that as the planting factor increases, the resonance shifts to lower frequencies and the peak is sharper. The result shown in Figure 5 contradict this rule (planting factors are 0.9 for Y and 1.1 for Z). Wave transmission is hindered by a poor contact of the sensor and the ground, i.e. only a fraction of the base area is in contact with the slab. In such conditions the transmissibility is governed by the motion of the mass of the sensor case (Drijkoningen 2000), and according to Washburn &Wiley (1941), the peak shifts to higher frequencies when the sensor weight decreases (as occurs with sensor Z).

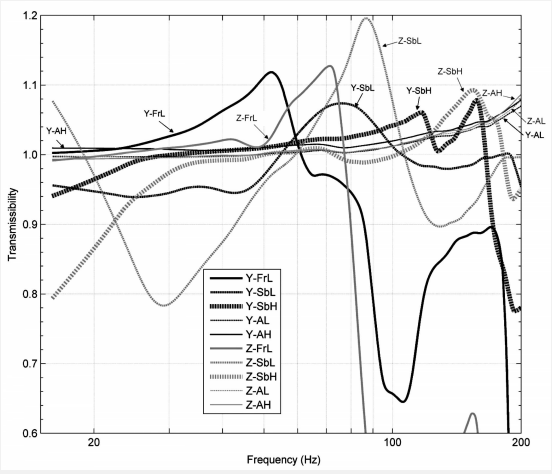

Figure 5. Coupling transmissibility of vibrations; the seismograph code (Y, Z) is given before the tests acronym (FrL: free at low velocities; SbL: sandbagged at low velocities; SbH: sandbagged at high velocities; AL: anchored at low velocities; and AH: anchored at high velocities).

3.4 Transmissibility of sandbagged sensors

The use of sandbags encompasses a more complex transmission of vibrations. In general, low and mid frequencies are damped and high frequencies amplified depending on the velocity level. For low velocities (SbL tests), the amplitude is damped from 16 to around 50 Hz up to 0.78 (-2.16 dB), and resonance occurs at 70-90 Hz (76 Hz for Y and 86.7 Hz for Z) with transmissibility between 1.07 and 1.2 (0.59 and 1.58 dB), respectively. In high velocity (SbH) tests, vibration damping occurs with less intensity and in a narrow frequency range. The resonance is shifted to roughly 155 Hz with a maximum transmissibility near the lower range of those from SbL, and the sensors follow the slab motion between 30 to 80 Hz. These results may be borne in variations in the bag positioning shown in Figure 2, rather than in the different vibration velocities of the slab. Other studies (Blair 1987, Khron 1984) show that an increase of ground motion affects in an opposite way to the resonant frequency than that observed here. Assuming that in SbL tests the contact is about 40 % of the bag surface and that in SbH, it is around 80 %, the planting factors are 0.66 and 0.33, which explain differences in the transmissibility curves from low and high velocity tests.

3.5 Measuring errors at different acceleration levels

In order to assess the measuring errors as function of the expected acceleration levels, the absolute value of the gain due to coupling, |GC| is considered. As no differences in the sensor mass or size are taken into account in the field, data from both seismographs are considered together for each coupling method. Accelerations are calculated for each measurement point from the peak velocity and the frequency, and associated with the local gain at that point. These data are classified according to ISRM (1992) and ISEE (2009) criteria into low (a< 0.2g), medium (0.2g≤a<1g), and high (a≥1g) acceleration. The distributions of |GC| values are plotted in Figure 6 for the three acceleration levels considered. They are displayed in the form of box plot for the mounting methods under evaluation: free, sandbagged, and anchored. An asterisk is written next to the coupling method to show that such technique is valid at those accelerations. Box plots display for each group of data: the first and third quartiles (upper and lower limits of the boxes); the median (central line); the lowest and highest values within 1.5 times the interquartile range (whiskers outside the box); and outliers (dots that are displaced along the abscissa to avoid overlap between points). The 95 % percentile of the absolute value of the gains is plotted as a solid circle.

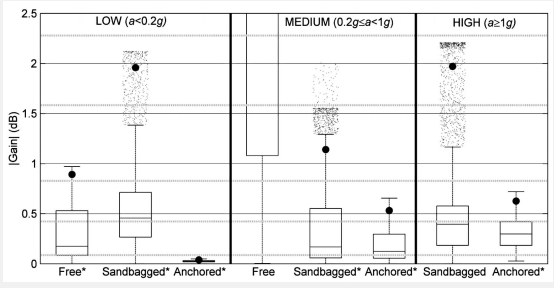

Figure 6. Distributions of the absolute value of the gain due to coupling at different acceleration levels (solid circles are the 95th percentiles; horizontal lines show a transmissibility of 1.01, 1.05, 1.1, 1.2 and 1.3; the asterisks next to the coupling method indicate the suitability of such method according to field guidelines)

Sensor anchoring has the highest accuracy and reproducibility. Errors are in general within the accuracy admitted for blasting seismographs (ISEE 2011), and they increase with the acceleration; the 95% $|G_C|$ is 0.62 dB (T≈1.07) at high accelerations. If the other methods are used at the suitable acceleration range, the median of the absolute value of the gains are acceptable, up to 0.46 dB (T≈1.05). The gains can be, however, much greater and the 95% percentiles of the absolute gains are 0.89 dB for free sensors (T≈1.11), and 1.14 dB (T≈1.14) for sandbagged sensors at low accelerations, and 1.96 dB (T≈1.25) for sandbagged sensors at high acceleration levels. Sandbagging provides the highest dispersion. If a method is applied outside the suggested range of accelerations, which in practice may occur as it is difficult to known a priori the acceleration levels at a monitoring point, the errors are out of control for free sensors and vary greatly when they are sandbagged. Errors shown in this work are in line with the uncertainties from quarry measurements with anchored (0.5

to 6.4 %) and sandbagged sensors (0.5-13.4 %) correctly oriented towards the blast (Segarra et al. 2012a).

4. CONCLUSIONS

Two blasting seismographs of different size, shape and mass were tested in a shaker table. A known horizontal periodic motion of constant amplitude and frequency from 16 to 200 Hz with a variation rate of 0.02 octaves /s was applied. The transmissibility of vibration is expressed as function of the frequency and calculated for the longitudinal geophone, that was aligned with the shaker axis. Transmissibility is computed from the spectral densities as the ratio of the longitudinal geophone output to the motion of the material in contact with the sensor (table or rock). It gives a quantitative statement of the total errors committed for the horizontal components (either longitudinal or transversal). Smoothing techniques have been applied to filter noise and retain the trend of data. The transmissibility of the sensors or baseline error is obtained from one test at 10 mm/s with the sensor anchored to the table (in which it is assumed that the coupling is perfect). It varies between 0.96 and 1.03 of the plate velocity (-0.35 to 0.26 dB). In 10 tests the sensors were laid over a grey granite slab attached to the table and coupled without a holding force, sandbagged or anchored. The input velocities of the slab were 5 mm/s for all coupling methods and 20 mm/s for sandbagged and anchored sensors. The total transmissibility is divided by the seismograph transmissibility in order to obtain the measurement error or transmissibility due to the coupling conditions. Though the transmissibility is site dependant, the results shown here give an insight to the performance of coupling methods commonly used to monitor vibrations on rock. The main findings are:

- Measurements with anchored geophones have the best accuracy, 1.02 times the input velocity (0.17 dB), in the common frequency range for blasting (frequencies below 100 Hz) and the smaller dispersion (the maximum transmissibility difference is less than 0.02).
- Measurements with the sensor freely placed on rock do not provide a good contact with the rock, and the amplitude response is governed by the sensor weight. Though the lighter sensor has a major risk of decoupling, it provides higher resonant frequencies (71.3 Hz versus 52.1 Hz) and a wider range in which errors are negligible (16-40 Hz versus 16-28 Hz). The transmissibility is similar for both and around 1.12 (0.98 dB). For frequencies above the resonant, the ground motion in the horizontal component is strongly damped by the sensor.
- When sensors are sandbagged, the transmission of vibrations is complex and the reproducibility is low. Poor planting (the weight over the sensor increases much more than the contact surface) provides bad records with a damping at 16 to around 50 Hz up to 0.78 (-2.16 dB), and transmissibility between 1.07 and 1.2 (0.59 and 1.58 dB), around 80 Hz. Better coupling (the weight increase is compensated by a large contact surface), shifts the resonance to 155 Hz, and leads to a frequency range from 30 to 80 Hz in which the sensors follow accurately the slab motion.

Three acceleration levels: low (<0.2g), medium (0.2g-1.0g) and high(>1.0g), have been defined to assess the error committed when common field practice guidelines are applied. The performance of the coupling methods at the different acceleration levels has been assessed from the absolute value of the gain. Data from both seismographs are considered together. The results show that:

- When the sensors are anchored, errors are ranged at low values at any acceleration level; the median and 95 % percentile are 0.30 and 0.62 dB (transmissibility of 1.04 and 1.07, respectively), respectively in the worst case.
- If a coupling method is applied outside the suggested acceleration range (e.g. sensor freely placed when accelerations are over 0.2g and sandbagged sensor at accelerations above 1.0g), which can likely happens in practice, the errors (absolute value of the gain) could be large (the 95 % percentiles are 12.6 and 1.97dB for free and sandbagged sensors, respectively).
- Though the median errors are up to 0.46 dB (transmissibility of 1.05), when a coupling method is applied within the suggested acceleration range (i.e. freely sensors at accelerations less than 0.2g and sensors held with a sandbag at accelerations below 1g), the errors can be high: 0.89 dB for free sensors (T≈1.11), and up to 1.96 dB (T≈1.25) for sandbagged sensors.

ACKNOWLEDGMENTS

The experimental work has been partially funded by MAXAM Civil Explosives and VIBRAQUIPO, which support is gratefully acknowledged.

REFERENCES

Adhikari, G. R., Theresraj, A. I., & Gupta, R. N. (2005), Influence of transducer-ground coupling on vibration measurements. *Fragblast*, 9(2), 79-92.

Armstrong, L.W. (2001), Evaluation of parameters affecting blast induced vibrations, *Ph. D Thesis.* Wollongong, Australia: University of Wollongong.

Armstrong, L. W., & Sen, G. C. (1999), The measurement of blast induced vibrations in soil. Proc. *EXPLO'99,* pp. 99-104.

AENOR (1993), *Control de vibraciones producidas por voladuras,* Norma UNE 22-381-93. Madrid: Asociación Española de Normalización y Certificación.

Blair, D. P. (1987), The measurement, modelling and control of ground vibrations due to blasting. *Proc. of the 2nd Int. Symposium of Rock Fragmentation by Blasting,* Keystone, pp. 88-101.

Blair, D. P. (1995a), Soil-embedded detector mounts for seismic monitoring. *Geophysics,* 60(1), 120-133.

Blair, D. P. (1995b), Blast vibrations in soil and on large resonant structures. *Proceedings Explo 95,* Brisbane, pp. 317-322.

BSI (1993), *Evaluation and measurement for vibration in buildings: Guide to damage levels from groundborne vibration,* BS 7385: part 2. London: British Standard Institution.

Cleveland, W.S. (1979), Robust locally weighted regression and smoothing scatterplots. *Journal of the American statistical association,* 74(368), 829-836.

DIN (1999), *Structural Vibration Part 3: Effects of vibration on structures,* DIN 4150-3:1999-02. Berlin: Deutsches Institut für Normung.

Drijkoningen, G. G. (2000). The usefulness of geophone ground-coupling experiments to seismic data. *Geophysics,* 65(6), 1780-1787.

Drijkoningen, G. G., Rademakers, F., Slob, E. C., & Fokkema, J. T. (2006), A new elastic model for ground coupling of geophones with spikes. *Geophysics,* 71(2), Q9-Q17.

Faber, K., & Maxwell, P. W. (1997), Geophone spurious frequency: What is it and how does it affect seismic data quality. *Canadian Journal of Exploration Geophysics,* 33(1&2), 46-54.

Farnfield, R.A. (1996), So you think you are monitoring peak particle velocity? *Proc.12th Symposium on Explosives and Blasting Research,* Orlando, pp. 13-17

Hoover, G. M. & O'Brien, J. T. (1980), The influence of the planted geophone on seismic land data. *Geophysics,* 45(8), 1239-1253.

Hutchison, W., Grigoryan, E. & Lorsbach, G. (2005), Significant sources of errors in the seismographs error budget. *Proc. 31st Annual Conf. on Explosives and Blasting Technique,* Orlando, FL.

ISEE (2009), *ISEE field practice guidelines for blasting seismographs 2009 edition.* Eltschlager K.K. (standards chairman committee). Cleveland: International Society of Explosives Engineers.

ISEE (2011), *Performance specifications for blasting seismographs.* Eltschlager K.K. (standards chairman committee). Cleveland: International Society of Explosives Engineers.

ISRM (1992), Suggested method for blast vibration monitoring. Dowding, C.H. (working group co-ordinator). *Int. J. Rock Mech. Min. Sci. & Geo. Abstr.,* 29(2): 143-156.

Krohn, C.E. (1984), Geophone ground coupling. *Geophysics,* 49(6), 722-731.

Segarra P., Sanchidrián, J.A., López, L.M., Querol, E. & Gutierrez, J. (2010), Assessment of the error of blast vibration measurements. *Proc. of the 9th Int. Symposium of Rock Fragmentation by Blasting-Fragblast 9,* Granada, pp. 551-560

Segarra, P., López, L. M. & Sanchidrián, J. A., (2012a), Uncertainty in measurements of vibrations from blasting, *Rock Mechanics and Rock Engineering,* 45(6): 1119-1126.

Segarra P., Sanchidrián J.A., López L.M. & Llamas A. (2012b), Measurement errors in vibrations from blasting. *Proc. of the 10th Int. Symposium of Rock Fragmentation by Blasting-Fragblast 10,* Delhi, pp. 349-356.

Singh, P.K. & Roy, M.P. (2010), Damage to surface structures due to blasting. I*nt. J. Rock Mech.& Min. Sci.*47(6): 949-961.

Siskind, D.E., Stagg, J., Kopp, J.W. & Dowding C.H. (1980), *Structure Response and Damage Produced by Ground Vibrations from Surface Mine Blasting,* USBM Report of Investigation 8507. Twin Cities: U.S. Bureau of Mines.

Stagg, M.S. & Engler, A.J. (1980), *Measurement of blast-induced ground vibration and seismograph calibration,* USBM Report of Investigation 8506. Twin Cities: United States Bureau of Mines.

Vázquez, P., Alonso, F.J., Esbert, R. M., & Ordaz, J. (2010), Ornamental granites: relationships between p-waves velocity, water capillary absorption and the crack network. *Construction and Building Materials,* 24(12), 2536-2541.

Washburn, H., & Wiley, H. (1941), The effect of the placement of a seismometer on its response characteristics. *Geophysics,* 6(2): 116-131.

Wheeler, R. (2004), The importance of proper seismometer coupling. Proc. of the Annual Conference on Explosives and Blasting Technique, Vol. 2, pp. 147-160.

Williams, A., & Treleaven, T. (2003), Trench blasting in close proximity to existing utilities in ultra metamorphic rock. *Journal of Explosives Engineering,* 20(4), 6-8.

Shock and Blast Behaviour of Confined Underwater Blasting Generators

J. Ambrósio[a], J. Gois[a] and J. Campos[a], P. Santos[b] ,
B. Duarteb and N. Oliveira[b], J. Pereira[c] and P. Lourenço[c]
[a]*LEDAP/ADAI - Lab. of Energ. and Det./Ass. for Dev. Ind. Aerod.*
Av. Univ. de Coimbra, 3150-277 Condeixa - PORTUGAL
[a]*Mech. Eng. Depart. - Fac. of Sciences and Technology, Polo II, Univ. of Coimbra*
[b]*CIEPQPF, bDep. of Chem. Eng., Fac. of Sc. and Tech, Polo II – Univ. of Coimbra,*
[c]*ISISE, cDep. of Civil Eng., University of Minho, 4800-058 Guimarães, Pt.*

Underwater blasting operations have been, during last decades, subject of research and development of maritime blasting operations, including torpedo studies. Aquarium tests, for the measurement of blasting energy of industrial explosives, are based in studies of confined underwater blast wave generators (WBWG). In a previous recent study it was presented the behavior of WBWG, based in water plastic containers, having in the center a detonator inside a cylindrical explosive charge, using an industrial ammonium nitrate emulsion explosive. The possible variation of composition and shock transmission lead to also use PETN (PentaErythritol TetraNitrate) charges form detonating cords. Prediction of detonation properties of emulsion explosives and PETN were done using thermochemical computer code, named THOR. Results were correlated with experimental values in order to get a more accurate prediction of detonating products expansion inside water of WBWG. These predictions, starting from THOR results allow to define and optimise JWL parameters. Autodyn® 3D predictions of WBWG, using a cubic meter water container, show the possibility of having charges without the immediately destruction of WBWG containers.

1 INTRODUCTION

1.1 Introduction

Underwater blasting operations have been, during last decades, subject of research and development of maritime blasting operations (torpedo studies and energy measurement of industrial explosives). The original blast wave generators (BWG), from the direct application of explosion in air of high explosives, have the inconvenient of hot polluted gases products, a reduced area of induced pressure, the possibility of generation of high velocity fragments and the existing of a very intense sound wave. Since physical properties of water and air are different, the characteristics of the shock waves (in air and water) are different principally due to the differences of density and shock wave velocity (shock impedance). Shock wave in water is 4.5 times faster than in air; pressure impulse in shock wave in water is 15-20 times higher than in air. After the detonation of an underwater explosive charge, the detonation products expand generating shock wave in water and forming a gas bubble. In our particular case, using small charges, the pulse bubble phenomena must be reduced or even eliminated. Our interest is to use water just as a pressure dissipative media.

1.2 Underwater blast wave generators

Several studies concern aquarium tests for the measurement of blasting energy of industrial explosives. Confined underwater blast wave generators (WBWG) then appear as an industrial application of reduced size aquarium test procedures. The confined WBWG, applying the extremely high rate conversion of the explosive detonation energy into the kinetic energy of a thick water confinement, allows a wide range of the produced blast impulse and surface area distribution. It also avoids the generation of high velocity fragments and reduces atmospheric sound wave. This kind of WBWG find an wide application in special anti-terrorist operations as an effective mean for breaching doors, walls, roofs or reinforced windows (Plaksin and Campos, 2007). This study shows the blasting effect of underwater detonations of 50 g charges of plastic bonded explosive inside the water-filled 50-litter container. After theoretical evaluation, the BWG has been tested in various experiments, revealing the shock sensitivity and the detonation wave performance of PBX charges, the shock wave attenuation in water and finally the interaction of the PBX driven water buffer with the obstacle mimic. More recently, the recent studies of WBWG open the possibility of collecting detonation products, specially condensed materials, from small explosive charges placed in the center of a water confinement, without the destruction of water container (Tavares et al., 2012).
The presented study shows the behaviour of WBWG, based in water plastic containers, having in the center a cylindrical explosive charge. In a previous recent study it was used an ammonium nitrate/fuel oil emulsion explosive (Ambrósio et al., 2013) as explosive charge. However, existing differences in experimented emulsion explosive detonation behaviour, due mainly to the life time of this kind of compositions, lead us to also use PETN - PentaErythritol TetraNitrate (a very well defined chemical component) as the explosive charge material.

2 DESIGN CONFIGURATIONS AND DIMENSIONS

2.1 Previous configurations

Plaksin and Campos, 2007, describe a simple design of BWG, which represents the 50g-charge of PBX based on RDX (Hexogen, C3H6N6O6) within the 50-litter (25 x 40 x 50 cm) polyethylene container filled with water. The 30-mm-thick aluminum bar joined with the 120-cm-long steel hollow bar, both integrated to the optical recording system (Plaksin et al., 2002, 2007) was applied as the obstacle stimulant. The analysis of velocity and momentum of motion, transmitted by the BWG to the obstacle, provides the way not only for the quantification of the BWG power but also for the optimization of the explosive charge design and its position inside the container. The chemical energy of an underwater explosion is partitioned between the “bubble” energy of gaseous detonation products, the water non-dissipated internal energy, part of shock energy dissipated in surrounding water to heat and the water kinetic energy. Sternberg

& Hurvitz, 1976, studied distribution of the explosive chemical energy at underwater detonation. Obtained results prove the quasi linearity of shock behaviour inside water.

2.2 Present configuration

Present configuration (Tavares et al., 2012, Ambrósio et al., 2013) uses a plastic cubic meter container (enclosed in aluminium thin tube net grid - Figure 1). Selected explosive is placed in the center of container using an aluminium 20 mm diameter tube (Figure 2).

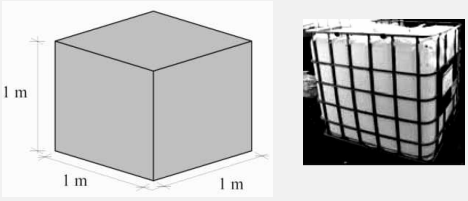

Figure 1. Plastic cubic meter container.

Figure 2. Aluminum tube having the small charge at the end.

A pressure sensor was (Ambrósio et al., 2013) glued to the container external wall for measuring the impact inflicted by the BWG (blast wave generator). The mechanism used to measure the pressure consists in an assembled instrumented stainless steel plate, between the ground floor and the water plastic container. The pressure set up is a pressure tube connected to a pressure sensor. This tube contains thin oil and is connected in a closed loop to a pressure transducer (Figure 3).

Figure 3. Experimental pressure set up - hydrostatic pressure transmission.

The pressure device measure the hydrostatic pressure level (Figure 4). Measured levels justified a 4-20 mA Gems® Sensors & Controls (3100 series). Both pressures were connected as a current output according with specifications. The electrical circuit and correspondent connections of the sensor to the periphery recording equipment are presented in Figure 4.

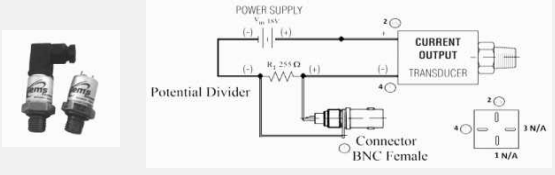

Figure 4. 3100 Series Pressure Transmitter, 4-20mA and its connection circuit.

The pressure sensores were calibrated for a source supply of 24VDC and a pressure level up to 6x105 Pa from compressing air, using a oscilloscope (Tektronix TDS 320) as periphery recording equipment (Ambrósio et al., 2013).

In order to dynamically calibrate pressure transducers procedure and to evaluate outside container blast pulse, some experiments were performed with 25 litter plastic containers (Fig. 5) having approximately 0.26x0.26x0.37 m. Explosive charge was placed in the center of the plastic container using a plate adapter, fixed in the open hole, or using a vertical plastic tube vertically fixed from the opening hole.

Figure 5. Plastic 25 litter container, charged with explosive, on the pressure set-up plate.

Selected explosive was (Tavares et al., 2012, Ambrósio et al., 2013) an ammonium nitrate-fuel oil emulsion explosive. The composition of emulsion explosive was presented in Table 1 and its detonation properties was presented in Table 2, according to THOR code predictions, as it will described latter (being Eo the Internal Energy, ao the sound velocity, u the particular velocity of detonation products and G its Gibbs Free Energy value).

Table 1. Main components and global characteristics of classical emulsions explosive

NAME	COM. NAME	REF	GLOBAL FORM.	DENS. [g/cm3]		COLOR	PHYS. STATE
				Bulk	Effective		
Ammonium Nitrate	Porous Am. Nit.	AN	NH_4NO_3	0.69-0.74	1.725	white	solid
Oil	Diesel Oil	Oil SAE 30	-	0.9		yellow	liquid
Microcristal Wax	Galp P1	Galp P1	-	-	-	white	solid
Parafin Wax	Guerowax -70	Guerowax -70	-	-	-	yellow	solid
Sorbitan Monooleate	Span 80	Span 80	-	-		yellow	liquid
Sorbitan Sesquioleate	Arlacel 83	Arlacel 83	-	-		yellow	liquid
Hollow Glass Microballons	Q-CEL 400	Q-CEL 400	-	0.11	0.21	white	solid

Table 2. Initial and predicted detonation products properties from emulsion explosive.

Initial conditions	**CJ conditions**	
Density ρ= 1112.13 kg/m^3	VoD=5480.88 m/s	T = 1988.493K
E_o=- 5619.53 kJ/kg	Pressure =8.102 GPa	G = -1.44E+04 kJ/kg
T = 298.15 K	a_o = 4151.77 m/s	γ = 1.22
Pressure =10^5 Pa	u = 1329.12 m/s	Γ = 3.12

Existing differences in tested emulsion explosive detonation behaviour, due mainly to the life time of this kind of compositions, it was decided to use also PETN - PentaErythritol TetraNitrate (a very well defined chemical component) as the explosive charge

material. According to open bibliographic information, PETN presents the followed properties:

Table 3. Global characteristics of PETN explosive.

NAME	COM. NAME	REF.	GLOBAL FORM.	DENS. [g/cm3]		Melting point	Boiling point
				Bulk	Effective		
PentaErythritol TetraNitrate	Pentrite	PETN	$C_5H_8N_4O_{12}$	0.69-0.74	1.77	142.9 C	180 C

3 APPLIED MODELS AND RESULTS

3.1 Detonation products properties

3.1.1. Thor predictions. The theoretical prediction of thermodynamic properties of detonation products of PETN, for Chapman-Jouguet detonation, was performed using THOR code. The THOR code have been developed and optimized for several kinds of equation of state (for example BKW, Boltzmann and JCZ3). Presented predictions used the EoS developed by Luísa Durães et al., 1995, HL, to calculate equilibrium compositions of gas and solid species, as a function of initial composition of energetic system, based on physical intermolecular potential of gas components. The selection of components is dependent of atomic initial composition. The code allows the possibility of estimating various sets of reaction products, obtained successively by the decomposition of the original reacting compound, as a function of the released energy. The following image represents the THOR structure of calculation (Figure 6).

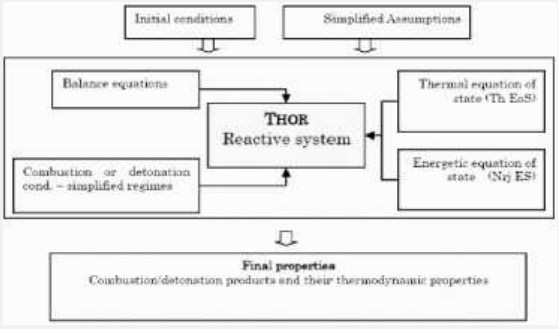

Figure 6. THOR structure of calculation.

The numerical calculation, using THOR code, was performed assuming a mixture of 99.958 % of PETN ($C_5H_8N_4O_{12}$) and 0.042 % of air ($N_{1.5788}O_{0.4212}$) in order to have an initial density close to the existing apparent density of the charge (1100 kg/m^3). Predictions assumed the equilibrium composition of detonation products of CO_2, H_2O, N_2, H_2, OH, CO, NH_3, O_2, NO, H, C(gas), N, O, C_α, C_β, CH_2O_2 species for the minimum Gibbs Free Energy - G. Detonation products properties of PETN, calculated by THOR code, were presented in Table 4.

Table 4. Initial and final detonation products properties using THOR code.

Initial conditions	CJ conditions	
Density ρ= 1100 kg/m^3	D_{CJ}= 5437 m/s	T = 3847 K
E_o= -1682.85 kJ/kg	P_{CJ} = 8.73 GPa	G = -2.59 E+04 kJ/kg
T = 298.15 K	a_{CJ} = 4057 m/s	γ = 1.1
Pressure =10^5 Pa	u_{CJ} = 1488 m/s	Γ = 2.63

3.1.2. JWL coefficients.

The obtained results, using THOR code for the calculation of adiabatic and isentrope expansion curves (from CJ point), are represented in Figure 7.

The isentrope curve was calculated for two ranges: the first one, nominated “restricted curve”, was calculated until expansion reaches a non dimensional volume ratio (until 14.29 times the initial CJ volume) and the second one, nominated “full curve”, for all the calculated expanded values. As it can be seen (Figure 7):

- the numerical power trend line approach shows, in the case of adiabatic curve the exponent of -2.602, in the case of restricted isentrope curve (for the main expansion zone) the exponent of -1.825, and for all values of isentrope curve the exponent of -1.356.

In fact, the first two curves (adiabatic and restricted isentrope curves) are quite approaching a linear evolution using a double logarithmic scale plot (vd. Figure 8) showing a global approach of a power trend line of exponent – 2.035 (vd. Figure 8).

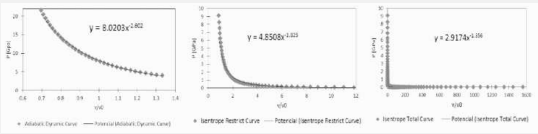

Figure 7. Evolution of predicted adiabate, restricted isentrope and full isentrope curves (P as a function of adimensional volume (v/vo), where).

The JWL equation of state (EoS) for expanded detonation products is expressed in the classical form

$$P_S(v) = Aexp\left(-R_1\frac{v}{v_0}\right) + Bexp\left(-R_2\frac{v}{v_0}\right) + C\left(\frac{v}{v_0}\right)^{-(\omega+1)}$$

where the exponent ω can be correlated to Gruneisen coefficient by $\omega = \Gamma - 1$ hen it can be expressed (vd. Handlev, 2011). The previous equation of pressure can be integrated for v varying from v_0 $(v_0 = v_{CJ})$ to its infinite value, giving a values that can be associated to the internal energy. This assumptions helps the definition of the other 5 coefficients (A, B, R_1, R_2 and C). From the Caroline, 2011, C parameter can be deduced by the energy released of the detonation products at a constant volume:

$$C = \frac{\omega \emptyset_{CJ}}{v_0} \quad (1)$$

Where $\emptyset_{CJ}$ is given by the next expression:

$$\emptyset_{CJ} = \int_{T_0}^{T_1} c_v\, dT = c_v[T_1 - T_0] \quad (2)$$

then,

$$C = \frac{\omega c_v[T_1 - T_0]}{v_0} \quad (3)$$

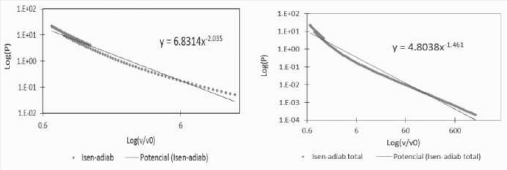

Figure 8. Evolution of predicted adiabatic and restricted isentrope curves ("Isen-adiab"), adiabatic and full isentrope curves ("Isen-adiab total") - (P as a function of adimensional volume (v/vo) if a double logarithmic scale, where $v_0 = v_{\square}$).

In our case, in order to calculated the JWL coeficients, a new numerical method was used. It was based in the evolution of adiabate and isentrope curves, obtained by THOR code, using a function of the Microsoft Excel ®, assuming a few assumptions (Table 5): (1) the Gruneisen coefficient from the exponential of the adiabatic curve ["*graphic results*" - res. 1.0 and 1.1] (Figure 9 and 10), (2) the Gruneisen coefficient from the exponential of the limit isentrope curve [res. 2.0 and 2.1] (Figure 11 and 12), (3) the Gruneisen coefficient from the exponential of the total isentrope curve [res. 3.0 and 3.1] (Figure 13 and 14) and, at last, (4) the Gruneisen coefficient and the parameter C of JWL deduced by Caroline (Handley, 2011)[res. 4.0] (Figure 15). The following graphics correlate graphically the theoretical curve, given by THOR code, to the predicted curve JWL for the different results: res. 1.0, 1.1, 2.0, 2.1, 3.0, 3.1 and 4.0.

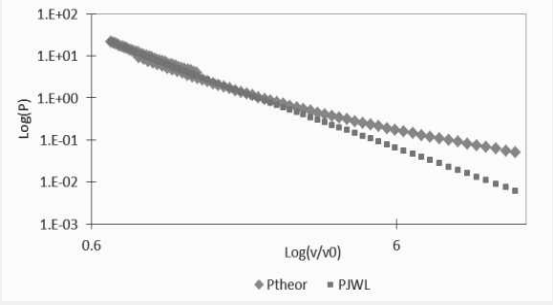

Figure 9. Adiabatic and restricted isentrope curves, at 1.602 Guneisen coefficient of the experimental curve, JWL - res. 1.0.

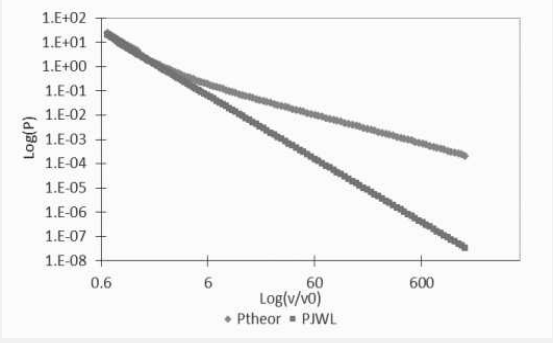

Figure 10. Adiabatic and full isentrope curves, at 1.602 Guneisen coefficient of the experimental curve, JWL - res. 1.1.

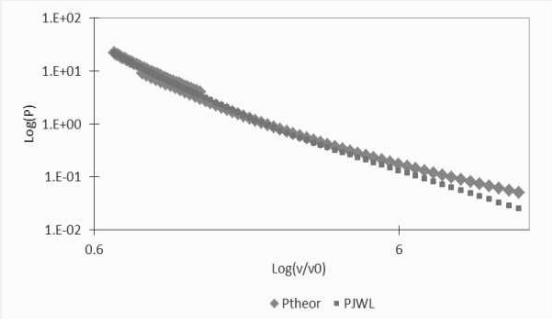

Figure 11. Adiabatic and restricted isentrope curves, at 0.825 Guneisen coefficient of the experimental curve, JWL - res. 2.0.

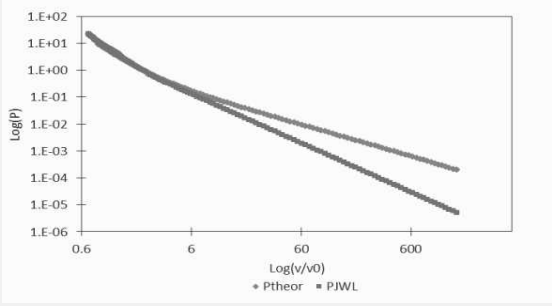

Figure 12. Adiabatic and full isentrope curves, at 0.825 Guneisen coefficient of the experimental curve, JWL - res. 2.1.

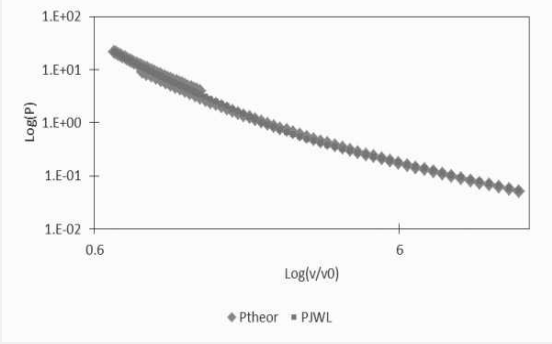

Figure 13. Adiabatic and restricted isentrope curves, at 0.356 Guneisen coefficient of the experimental curve, JWL - res. 3.0.

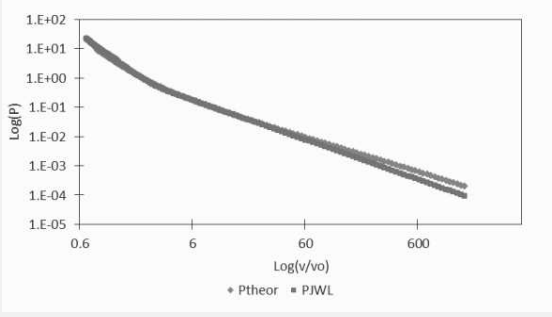

Figure 14. Adiabatic and full isentrope curves, at 0.356 Guneisen coefficient of the experimental curve, JWL - res. 3.1.

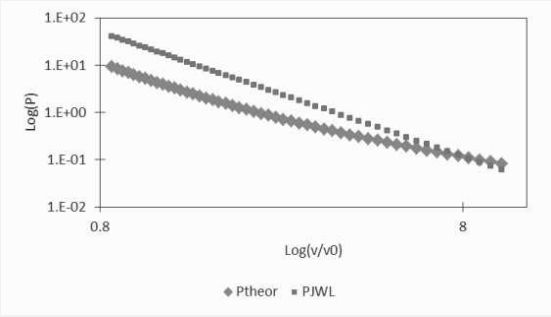

Figure 15. Adiabatic and restricted isentrope curves, at 1.63 Guneisen coefficient and at 27.56 GPa C parameter until 10 adimentional volume, from Caroline, 2011, for the experimental curve, JWL - res. 4.0.

Table 5. Calculated JWL coefficients according presented restrictions.

Test	ω	C	A	R1	B	R2	Deflection
		GPa	GPa		GPa		Σ [Ptheor.-PJWL]^2
1.0	1.602	6.81	800	8.29	50	5	26.93
1.1	1.602	6.81	1000	8.29	30	5	26.4
2.0	0.825	3.44	2486.75	8.2	41.54	2.59	25.5
2.1	0.825	3.44	2467.53	8.19	41.48	2.592	25.508
3.0	0.356	1.99	2354.65	7.93	47.78	2.385	25.421
3.1	0.356	1.99	2343.62	7.92	47.62	2.383	25.421
4.0	1.63	27.56	10	12	10	12	576

The presented results show the strong influence of exponent ω on the inclination deep of the curves.

3.2 Dynamic simulations

3.2.1. General equations. Basic general conservation equations are useful because they help to define quantities and design values of experiments. The first value is the pressure level DP, as a function of distance radius r related to the original radius of explosive charge r_0 (vd. Suceska, 2007), where A represents the products detonation pressure value (A=37 GPa for TNT of initial r=1600 kg/m^3) or the shock polar interaction between explosive expansion and water, and *a*=1.5 as a mean value of dissipation exponent:

$$\Delta p = A\left(\frac{r_0}{r}\right)^{\alpha} \qquad (4)$$

The pressure profile, as a function of time (vd. Fig. 16), can be expressed by equation 1.5 when $t < \theta$, and by equation 1.6 when θ <t< 5xθ to 10xθ, being $\theta = B_1\left(\frac{r}{r_0}\right)^{\beta}\frac{r_0}{c_0}$. The q is so-called time constant or characteristic P width of peak (it describes exponential pressure drop with time, and it is the P width value at which maximum pressure decreases to value p_{max}/e - vd. Suceska, 2007).

$$p(t) = \Delta p^{-t/\theta} \qquad (5)$$

$$p(t) = \Delta p 0.368^{\frac{\theta}{t}} \qquad (6)$$

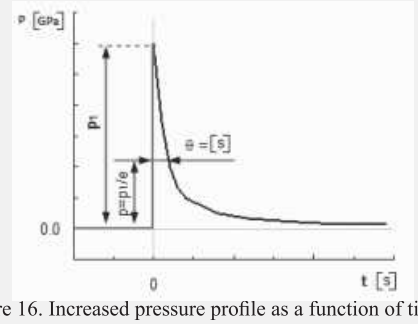

Figure 16. Increased pressure profile as a function of time.

These expressions allow to us to define limit dimensions for our designed WBWG. Detonation products properties of PETN explosive, calculated as a function of initial density, allow the determination of its detonation products shock polar. Detonation velocities were calculated using the D=1.608 + 3.933 r_0 (D given in km/s and r_0 in kg/dm^3) given by LASL, 1980. Obtained experimental pressure P were the values presented by Francis Ree, 1984. Acoustical approach from detonation products of PETN to the shock polar pressure of water allow the calculation of A=5.12 GPa for the initial density of PETN of 1170 kg/m^3. Assuming preceding A value and the *a*=1.5 value it was possible to determine transmitted shock pressure inside water container, as a function of radius distance from central charge (Figure 17). The obtained results seem to show the possibility to reach low final pressure values (P < 0.6 MPa) according to the previous experiments (Ambrósio et al., 2013).

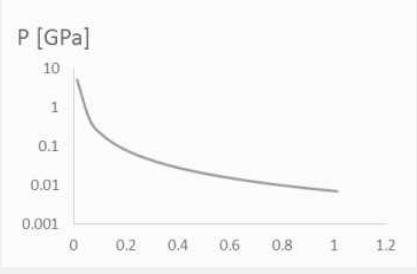

Figure 17. Peak pressure P [GPa] evolution as a function of radius r [m], from central charge.

3.2.2. Autodyn simulations. Autodyn® (Autodyn Ansys, 2006) simulations are performed in two separated and complementary configurations: (i) detonation progression inside cylindrical charge of 2.5 cm diameter and 2.1 cm long in 2D simulation, and (ii) expansion of detonation products inside a cubic meter water tank in 3D simulation, started from previous pressure and impulse levels obtained in 2D simulation. The second visualization (3D) was performed according the following scheme (Figure 18), where it can be seen the placement the charge inside cubic water tank. The pressure lines were vizualized, inside water, from the axial line of the charge. The configurations were assumed for 15.5 g PETN (with a density of 1.5g/cm^3) and for JWL parameters from Autodyn® data (A = 625.3 GPa, B = 23.29GPa, R1 = 5.25, R2 = 1.6, and 0.28). At CJ point DCJ = 7450 m/s , PCJ = 22GPa and ECJ = 8.56E+6 KJ/m^3.

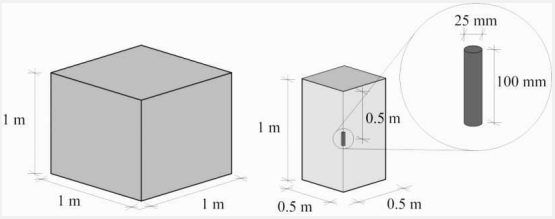

Figure 18. 3D Autodyn simulation scheme – properties were visualized by the faces generated in the vertival axial line of the charge.

Assuming a 2D configuration, it can be assumed that detonation wave travels through the explosive material from left to right (Figure 19). The shock front is followed by the chemical reaction zone. Behind the reaction zone are located the dense and hot gases from the detonation products. The increase the volume of the gases of the products generates an increase of the pressure, generating a shock wave inside surrounding material (water).

Figure 19. Simulation of propagation scheme of detonation of emulsion explosive.

The presentation of results concerns five particular instants: when detonation of explosive is at the end (2D simulation – Figure 20), when expansion products took the value 165 v/v0 of non-dimensional volume of (3D simulation – Figure 21 left), when expansion products touch the wall of water tank (3D simulation – Figure 21 center) and when expansion products in moving to the corners (3D simulation – Figure 21 right). For both simulation, 2D and 3D, it were measured the evolution at pressure, as a function of time, at two specific points that are identify on the bottom of their simulations (2D simulation – Figure 22 measure at point #1 and #2; and 3D simulation – Figure 23 measure at point #3 and #4).

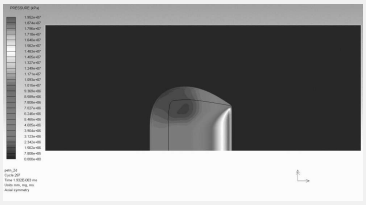

Figure 20. Simulation of detonation of emulsion explosive at its end (2D)

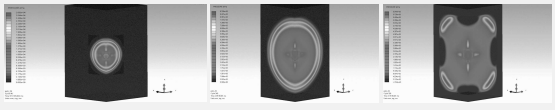

Figure 21. Simulation 3D of expansion products of detonation of emulsion explosive, when its non-dimensional volume reachs the value of 165 v/vo (3D simulation - left), when touch water tank wall (3D simulation - center) and when is moving to the corners zone (3D simulation - right).

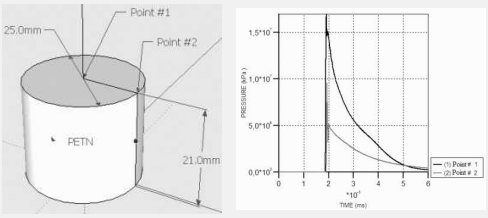

Figure 22. Pressure measurement at point #1 and #2 for the 2D simulation on the right. (The points are identify on the left picture and correspond to the extreme of the explosive, one measure on the center, Point #1, and other on the edge, Point #2).

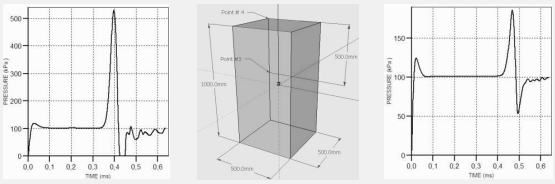

Figure 23. Pressure measurement at point #3, on the left, and point #4, on the right for the 3D simulation. (The points are identify on the center picture and correspond to the corner of the water container, one measured in the middle, Point #3, and other on the top, Point #4).

When the wave reaches the lateral container wall, according to presented simulations, a reflection wave is then generated, deforming the lateral wall under a sinusoidal shape. The corners, at this time, are not yet attained by the original positive wave (Figure 24). Consequently the lateral wall is deformed but not yet ruptured by the increasing internal pressure.

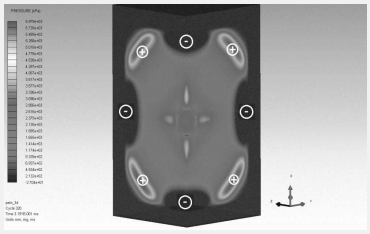

Figure 24. 3D simulation of pressure evolution inside water container.

Prediction pressure pattern shows levels of initial values of 19.52 GPa (at the end of detonation), 265E+5 Pa at expansion value of 165 v/vo, 87.58E+5 Pa when pressure front touch water tank wall, 59.79E+5 Pa when it touch corner zone and 50.45E+5 Pa when starts reflection from the corner. Selected points present the maximum value of 17 GPa at point #1, the maximum value of 9.5 GPa at point #2, the maximum value of 5.33E+5 Pa at point #3 and maximum value of 1.89E+5 Pa at point #4. Consequently it will be possible to keep the deformed plastic wall not ruptured during the first miliseconds of the experiences.

4 EXPERIMENTAL VALIDATIONS

4.1 Previous results – emulsion explosive blasted in plastic cubic meter containers

Previous study (Ambrósio et al, 2013) presented blast effect of 5 g, 10 g and 15 g study of ammonium nitrate-fuel oil emulsion explosive inside the cubic meter container (Figure 25). The plastic confinement was enclosed inside an aluminum net structure. The inlet opening of plastic cubic container was kept open, in order to have release opening pressure after initial shock and reflections (this cumulative process helps pressure decrease). Explosive aluminium support tubes deformation (after detonations) gives an idea of the pressure level, as a function of charge radius distance (vd. Figure 25). Recorded movies, at 1000 frame/s, also presents external deformation of plastic container and observed reflections (vd. Figure 25).

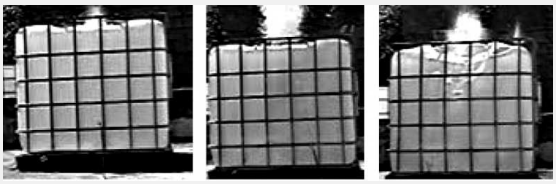

Figure 25. External deformation of plastic container and observed reflections for the 3 tested charges of emulsion explosive (5g left, 10g center and15 g right).

From these results it can be observed that detonation of small charges generate elastic deformation of plastic wall, without any permanent deformation. Four reflection shock movements of plastic container are clearly observed with 10 g charge. 15 g charge generates permanent deformation – all the other charges generate elastic deformation. Keeping inlet open allows a dissipative pressure decreasing process, observed clearly under 15 g charge - it allows the non-destruction of container. The non-destruction of cubic plastic container, designed for nominal pressure of 6 MPa, proves the validity of selected coefficients, design assumptions and simulation process.

4.2 Present results – PETN explosive blasted in 25 litter containers.

Present experimental study shows the deformation and blasting of 25 litter container for 2 classes of different explosive charges:
- using only the standard detonator (0.6g PETN charge + primary explosivey0.8 g of PETN) without any supplementary charge,
- using the same conditions of the previous test, but now adding 3g PETN (from a detonating cord) to the standard detonator.

All the experiments were recorded with a fast camera under 420 fps or 1000 fps sequences. Pressure were also measured and recorded. Pressure signal presents the classic pressure profile of this kind of experiments.

Fast video frames (at 420 fps sequence) of the first class of tests (only with the detonator charge) is presented in Figure 26.

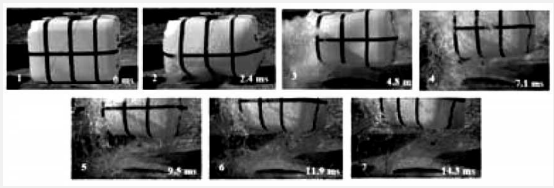

Figure 26. Video frames from first class of tests, using standard detonator as charge, inside a 25litter water container.

Fast video frames (sucessively at 420 fps and 1000 fps sequences) of the second class of tests (detonator more 3 gr of PETN) are presented in Figures 27 and 28.

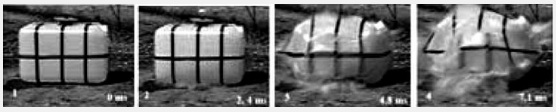

Figure 27. Video frames from second class of tests, using standard detonator more 3g of PETN as charge, inside a 25litter water container (420 fps sequence).

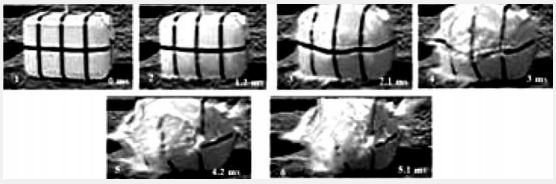

Figure 28. Video frames from second class of tests, using standard detonator more 3g of PETN as charge, inside a 25litter water container (1000 fps sequence).

Obtained results prove the validity of simulations, confirming central blasting phenomena process for the generation of an exterior blast generator. Main blast wave expands initially according an “equatorial” disc. The blast process, latter on, is expanding for all directions. Sinusoidal shapes of lateral walls were observed. Measured pressure levels are lower than theoretical expected values. Plastic 25 litter containers are ruptured at final, but not destroyed, confirming predicted values.

5 CONCLUSIONS

The present study shows the behaviour of WBWG, using water plastic containers, having in the center a cylindrical explosive charge. The used explosives were ammonium nitrate-fuel oil emulsion explosive and PETN. It was used a computer program, THOR code, to obtain the theoretical properties of the detonation products of used explosives. The theoretical predictions were adjusted to an evolution expansion curve using JWL parameters. Good adjustment (between the theoretical adiabatic and isentropic curves, from CJ point, obtained by THOR code, and predicted expansion curve using JWL equations) allows to define and optimise JWL parameters, under different restricted conditions. Gruneisen coefficient of 0.356 reveals to be a very good compromise value. Previous Autodyn® predictions of WBWG, using a cubic meter water container, show the possibility of having emulsion charges without destruction of WBWG containers. New series of experiments were performed

using 25litter plastic containers for different specific amounts of PETN, for the better understanding the interaction between the explosive charge and the water container. It is always observed the elastic deformation of containers wall, under the water shock reflections, changing from its original cubic shape to a transient spherical one. Obtained results prove the validity of simulations, confirming central blasting phenomena process for the generation of an exterior blast generator. Plastic 25 litter containers are ruptured at final, but not destroyed, confirming predicted pressure values.

Acknowledgements: *This work was performed under Project CH-Secure of Portuguese Foundation of Science and Technology – FCT. The authors acknowledge the support for this work.*

6 REFERENCES

Ambrósio, J., Ferreira, R., Mendes, R., Campos, J., Santos, P., Duarte, B., Oliveira, N., Pereira, J., Lourenço, P., 2013. "Prediction and experimental results of confined underwater blasting generators", in *Proc. of the 44th International Annual Conference of Fraunhofer ICT,* Fraunhofer-Institut für Chemische Technologie (Ed.), D. W. S. Werbeagentur und Verlag GMbH, Karlsruhe, Germany.

AUTODYN ANSYS, "Explicit software for non -linear dynamics", Manual, 2006.

Durães, L., Campos, J., Portugal, A. (1998), "Reaction Path of Energetic Materials Using THOR Code", in *Shock Compression of Condensed Matter-1997,* Part 1, Schmidt, S. C., Dandekar, D. P., Forbes, J. W. (Eds.), of AIP Conference Proceedings Series, Vol. 429, American Institute of Physics, Woodbury (NY), p.341-344.

Durães, L., Campos, J., Portugal, A. (2000), "Thermodynamical Prediction of Combustion and Detonation Properties Using Modified THOR Code", in *Proc. of the 27th International Pyrotechnics Seminar,* Grand Junction (CO), IIT Research Institute, Chicago (IL), USA, p.55-66.

Handley, Caroline A., 2011. "Numerical modelling of two HMX-based plastic-bonded explosives at the mesoscale", PhD Thesis, University of St Andrews.

Hansson, Hankan, 2009. "Determination of properties of emulsion explosives using cylinder expansion tests and FEM simulation", Swebrec Report.

LASL Explosive Property Data, 1980." Los Alamos Scientific Laboratory Series on Dynamic Material Properties", University of California Press.

Plaksin, I., and Campos, J., 2007. "Blast Wave Generator Based on PBX Enclosed in Water Container", in *Proc. of the 5th European Symposium on Non-Lethal Weapons,* Ettlingen, Fraunhofer-Institut für Chemische Technologie (Ed.), D. W. S. Werbeagentur und Verlag GMbH, Karlsruhe, Germany.

Plaksin, I., J. Campos, P. Simoes, A. Portugal, J. Ribeiro, R. Mendes and J. Gois., 2002."Detonation Study of Energetic Micro-Samples", in *Proc. of 12th Symp. (Int.) on Detonation,* San Diego, CA, 11-16 Aug., pp. 42-50.

Plaksin, J. Ribeiro, R. Mendes, and J. Campos, 2007. "Detonation Performance and Shock Sensitivity of PBX-s", in *Insensitive Energetic Materials – Particles, Crystals, Composites,* edited by Ulrich Teipel and Michael Herrmann. Fraunhofer IRB Verlag, ISBN 978-3-8167-7328-3. Pp 156-186.

Ree, F. H., 1984. "A statistical mechanical theory of chemically reacting multiphase mixtures: Application to the detonation properties of PETN", J. Chem. Phys. 81, pp. 1251.

Sternberg, H. M. & Hurvitz, H. , 1976. Proceedings *of Sixth International Detonation Symposium,* p 528.

Suceska, M., 2007. "Detonation", in *Proc. of 4th Workshop on Pyrotechnics Combustion Mechanisms,* Fraunhofer-Institut für Chemische Technologie, Karlsruhe, Germany.

Tanaka, K., "Detonation Properties of Condensed Explosives Computed Using the Kihara-Hikita-Tanaka Equation of State", *Report from National Chemical Laboratory for Industry,* Ibaraki, Japan, 1983.

Tavares, B., Mendes, R., Campos, J., Santos, P., Duarte, B., Oliveira, N., Lagoa, A., Antunes, E., Silva, S., Calado, J., 2012. "Kinetic thermo mechanisms of ceramic formation from detonation of metal/nitrated compositions", in *Proc. of Kishem Symposium,* Seul, Korea.

Tavares, B., Mendes, R., Plaksin, I., Campos, J., Santos, P., Duarte, B., Oliveira N., Pereira, J., Lourenço, P., 2012. "Prediction and experimental results of confined underwater blasting generators", in *Proc. of Kishem Symposium,* Seul, Korea.

Prediction of fragmentation from fracture toughness and brittleness for class II rocks

Victor A. Akinbinu
School of Mining Engineering, University of the Witwatersrand, Johannesburg, South Africa

ABSTRACT: This work studied the prediction of fragmentation from fracture toughness and brittleness. Fragmentation prediction is important as it affect the overall mining process. The post failure moduli of the rocks were determined with the use of a closed-loop servo-controlled testing machine. The brittleness index k proposed by Tarasov and Potvin (2013) was used to determine the brittleness of the rocks. The fracture toughness values of rocks were determined according to ISRM recommendation using cracked chevron notched Brazilian disc (CCNBD) specimens. The fragmentations are determined through image analysis of the muck pile. A regression analysis is used to correlate the blasting geometric ratios, powered factor, and brittleness index and fracture toughness with the mean fragmentations. The regression is significant and the coefficient of determination is 0.970. A further sensitivity analysis shows that fracture toughness and brittleness influences fragmentation more than powder factor and S/B ratio after H/B and D/B ratios.

1. INTRODUCTION

The fragments sizes distribution produced during blasting depends to a large extent on the energy available to cause fragmentation (from explosive) and the brittleness of the rock. In the literature it appears that no research attempted to link brittleness and fragmentation and the self-sustaining failure behaviour of rocks at post peak region. Rock failure under dynamic loading conditions as experienced in blasting, rockbursting, and the resulting fragments size distribution is a little-understood phenomenon. The ductility or brittleness of the rock has a significant effect under such loading conditions and the fragments that result.

There is at present no satisfactory theoretical basis for predicting dynamic failure behaviour while such a prediction can be very useful in the solution of many practical mining and civil engineering problems. For example, effectiveness of all the subsystems in the mining operation (e.g. Loading, hauling and crushing) is dependent on the optimal fragmentation quality prediction (production of fines and oversize of fragmented rocks impose problems); as well as rapid mining of ore bodies, design of stable structures and the efficiency of rock fragmentation processes can be designed and evaluated with more accuracy. Fragments sizes distribution of blasted rock is influenced by many factors group as the controllable and uncontrollable parameters: rock properties, explosive related property, and blasting patterns. Hence optimal prediction of particle sizes distribution of blasted rock is a very complex issues therefore no single method or equation can predict the blast fragmentation exactly. This research considered partitioning fragmentation models for Class I and Class II rocks. Since the response of both Class I and Class II rocks differs under static and dynamic loading conditions while Class I is ductile, the Class II are much brittle. Fragmentation of Class II rocks are energy efficient process as result of its self-sustaining fracturing behaviour, the Class I rocks on the other hand are energy intensive process as much of the energy are used in plastic deformation process ahead of breakage. Therefore the partitioning of fragmentation model into Class I and II will allow to determined the energy delivered by explosive and better prediction of fragmentation. As a result this research proposes a fragmentation model for Class II rocks.

The Kuz-Ram model considered as the generalised model for predicting fragmentation make use the uniaxial compressive strength (UCS) and the Young's modulus (E). Even though the fracturing of rock is usually due to tensile failure, no current blasting models consider it. Fractures and fragmentation of rocks are propagated through crack growth and coalescence. Fracture toughness which is the resistance of rock to fracture propagation and brittleness which is simply the ease of fracture to propagate better describe fragmentation than the UCS and E. It has also been shown than fracture toughness has a relationship with the tensile strength of rock, UCS and E as contain in Whittaker et al. (1992).

Wawersik and Fairhurst (1970) classified rocks into Class I and Class II according to their failure behaviour in a uniaxial compression test. Beyond the post peak region, either the curve continuously increases in strain or it does not. If it increases in strain, it is Class I; if it does not then it is Class II.

Tarasov and Potvin (2013) classified brittleness on a monotonic scale of Class I and Class II based on the capability of the rock to self-sustaining failure. The brittleness quantification depends on the stored elastic energy available in the post failure region to fragment the rock. It is obvious from Figure 1 that Class I and II rocks differs in brittleness hence the more brittle the rock the more fragments that are produced. Brittleness k is estimated based on the following equations:

$$k = \frac{dw_r}{dw_e} = \frac{E - M}{M} \tag{1}$$

Where,

$$dw_r = \frac{d\sigma^2(E - M)}{2EM}$$ is the rupture energy (2)

$$dw_e = \frac{d\sigma^2}{2E}$$ is the accumulated elastic energy available for rupture process (3)

$$E = \frac{\partial\sigma}{\partial\varepsilon}$$ is the unloading elastic modulus (4)

$$M = \frac{\partial\sigma}{\partial\varepsilon}$$ is the post-peak modulus in Figure 2.38b (5)

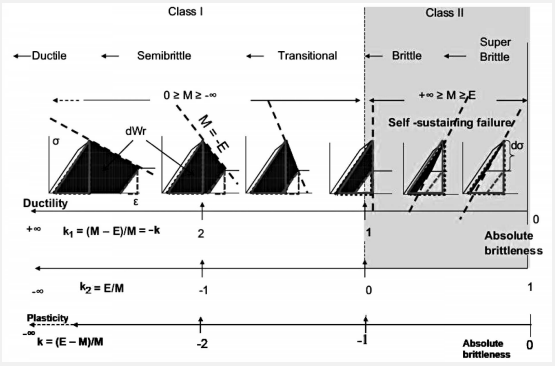

Figure 1. Scale of rock brittleness index, with brittleness increasing from left to right (after Tarasov and Potvin, 2013).

Apart from Kuznetsov (1973) model other several researchers have developed empirical techniques to predict the rock fragmentation. These include Cunningham, (1983) and Hjelmberg 1983. Several other researchers have also used multivariate analysis techniques in predicting blasting fragmentation. Hudaverdi et al. (2010) used multivariate analysis procedures for prediction of blast fragmentation. Monjez et al. (2009) used multivariate relation to predict rock fragmentation based on the main data (300 datasets). But such techniques which are based on the data acquired from different blasting operations, in an unclassified rock types (either Class I or Class II) may be misleading for generalised various rock brittleness conditions.

Sanchidrian et al and many other authors have used Image analysis software to measure the fragmentation of the quarry blasts. Gheibie et al. [25] have used image analysis software to determine particle size distribution of the blasts in Sungur Copper Mine. The examination and comparison of several image analyses software have been made by Latham et al. [23]. Hall and Brunton [26] have used image analysis software and compared the validity of blast fragmentation models developed in JKMRC.

2. METHODS

The fracture toughness (mode I) was determined using chevron notched short rod according to International Society of Rock Mechanics suggested methods (ISRM, 2007). The post failure modulus was determined for the rocks according to ISRM (2007). The fragmentation was quantified from the quarry blast using image sampling and analysis software (Split). The blasting geometric is estimated as ratio of spacing to burden (S/B), bench height to burden (H/B) and blasthole diameter to burden (D/B). These ratios have been the usual practice in blasting design and prediction. The relationship between fragmentation and brittleness estimated using equation1 with fracture toughness and blasting parameters were investigated through multivariate analysis. A further analysis was done using probabilistic analysis to investigate the influence of the various parameters on mean fragments size from the muck pile. The result is presented in the following session.

3. RESULTS AND DISCUSSION

3.1 Multivariate analysis

Table 1 show all the variables used in the analysis and their descriptive statistic. Table 2 shows the coefficients of correlation with fragmentation. From the table brittleness k, [(E-M)/M] has strongest correlation coefficient of 0.804 with fragmentation followed by powered factor and fracture toughness with correlation coefficient of 0.722 and 0.505 respectively. These parameters are significantly correlated with fragmentation (with significant value of $p \leq 0.05$).

Table 1. Descriptive statistic of the data.

	Mean	Std. Deviation
X50 (m)	.175120	.0609381
Kic (MPa*m^0.5)	1.619500	.1682377
S/B	1.014679	.0968141
H/B	4.491356	1.2152266
D/B	.002767	.0006125
pf (Kg/m3)	.448894	.2617687
(E-M)/M	-.170305	.0407027

Table 2. Coefficients of correlation and significant values of the data.

		X50 (mm)	Kic (MPa*m^0.5)	S/B	H/B	D/B	pf (Kg/m3)	(E-M)/M
Pearson Correlation	X50 (m)	1.000	-.505	-.172	-.494	-.404	-.722	-.804
	Kic (MPa*m^0.5)	-.505	1.000	-.690	.575	.255	.382	.522
	S/B	-.172	-.690	1.000	-.322	-.056	.213	-.015
	H/B	-.494	.575	-.322	1.000	.936	.282	.784
	D/B	-.404	.255	-.056	.936	1.000	.201	.719
	pf (Kg/m3)	-.722	.382	.213	.282	.201	1.000	.715
	(E-M)/M	-.804	.522	-.015	.784	.719	.715	1.000
Sig. (1-tailed)	X50 (mm)	.	.047	.296	.051	.097	.004	.001
	Kic (MPa*m^0.5)	.047	.	.007	.025	.212	.110	.041
	S/B	.296	.007	.	.154	.432	.254	.481
	H/B	.051	.025	.154	.	.000	.187	.001
	D/B	.097	.212	.432	.000	.	.265	.004
	pf (Kg/m3)	.004	.110	.254	.187	.265	.	.004
	(E-M)/M	.001	.041	.481	.001	.004	.004	.

The model summary in Table 3 shows the coefficient of determination of 97.0 % and that about 94.1 % of the variation in fragmentation is explained by the model 1 with the parameters used as the predictors. From the summary table, the standard error of estimation is low (0.02188) and a high significant value of 0.006.

Table 3. Model summary.

Model	R	R Square	Adjusted R Square	Std. Error of the Estimate	Change Statistics				
					R Square Change	F Change	df1	df2	Sig. F Change
1	.970*	.941	.871	.0218848	.941	13.381	6	5	.006

a. Predictors: (Constant), (E-M)/M, S/B, D/B, pf (Kg/m3), Kic (MPa*m^0.5), H/B

b. Dependent Variable: X50 (m)

Table 4 is the coefficients of the equation describing the relationship of the predictor with the outcome. The values of the partial correlations of the predictors rise sharply from the zero-order correlation. This means, for example, that much of the variance in the predictors cannot be explain by other variables. The tolerance is the percentages of the variance in a given predictor that cannot be explain by the other predictors. Thus, the high tolerance shows that above 80% of the variance in brittleness and fracture toughness cannot be explained by the other predictors. In addition both correlation of brittleness

and fracture toughness with fragmentation are quite significant (with p≤0.05). Therefore brittleness and fracture toughness are useful parameters for prediction of mean fragmentation of a muck pile size distribution. The model gives a good prediction of fragmentation. The equation of prediction is expressed below.

$$X_{50}(m) = 2.731 - 1.749K_{ic} - 0.061 S/B + 0.638 H/B - 1032.587 D/B - 0.102\rho - 1.671k \quad (6)$$

Table 4. Coefficient for the equation.

Model		Unstandardized Coefficients		Standardized Coefficients			Correlations		
		B	Std. Error	Beta	t	Sig.	Zero-order	Partial	Part
1	(Constant)	2.731	.798		3.420	.019			
	Kic (MPa*m^0.5)	-1.749	.582	-4.828	-3.007	.030	-.505	-.802	-.326
	S/B	-.061	.216	-.098	-.284	.788	-.172	-.126	-.031
	H/B	.638	.252	12.722	2.533	.052	-.494	.750	.274
	D/B	-1032.587	416.925	-10.379	-2.477	.056	-.404	-.742	-.268
	pf (Kg/m3)	.102	.057	.439	1.795	.133	-.722	.626	.194
	(E-M)/M	-1.671	.532	-1.116	-3.140	.026	-.804	-.815	-.340

a. Dependent Variable: X50 (m)

A residual is the difference between the observed and model-predicted values of the dependent variable. The residual for a given product is the observed value of the error term for that product. A P–P plot of the residuals in Figs. 1 will help check the assumption of normality of the error term. The P–P plot residuals should follow the 45° line. The P–P plot indicates that the normality assumption is not violated. The plot of residuals by the predicted values shows that the variance of the errors is a good scatter.

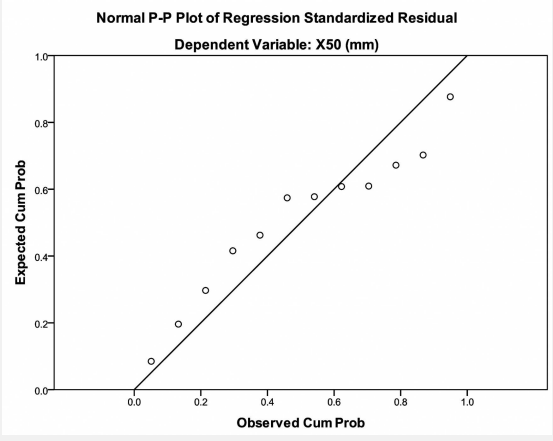

Figure 1. Normal P-P plot of regression standardised residual.

3.2 Stochastic analysis

Know fully that rocks and rock properties are heterogeneous and associated with uncertainty in its determination. A probabilistic analysis using Monte Carlo simulation is done. The simulation process model a series of random data of the parameters used in the prediction by calculating ten thousands of scenarios of the mean particle size prediction of the probability of different outcomes occurring. These variables were each modeled using probability distributions in Table 5 as input parameters. The output model, the mean fragmentations are shown in Figure 3 and 4 while output of the probability distribution model of the result, mean fragmentation is shown in Figure 6. A histogram and the cumulative plot of the output in Figure 3 and 4 check the assumption of normality of the error term in the outcome. The shape of the histogram should approximately follow the shape of the normal distribution curve. This histogram is acceptably close to the normal curve. The cumulative plot should follow the 45° line. Neither the histogram nor the cumulative plot indicates that the normality assumption is violated. The plot of residuals by the predicted values shows that the variance of the errors is a good scatter.

Table 5. Input data for the simulation.

Name	Graph	Min	Mean	Max	5%	95%
Kic (MPa*m^0.5)	0.8 2.2	0.9642427	1.619712	2.191194	1.341823	1.89708
S/B	0.6 1.4	0.6850145	1.015115	1.340409	0.8556129	1.178248
H/B	0 10	0.2789843	4.494382	9.07725	2.492469	6.502771
D/B	0.0005 0.0055	0.000579241	0.002770326	0.005078671	0.001777817	0.0037743
pf (Kg/m3)	-1.0 1.5	-0.6831121	0.4450026	1.46543	0.01856153	0.8631175
(E-M)/M	-0.35 0.00	-0.3234654	-0.1706185	-0.02472234	-0.2370981	-0.1036816

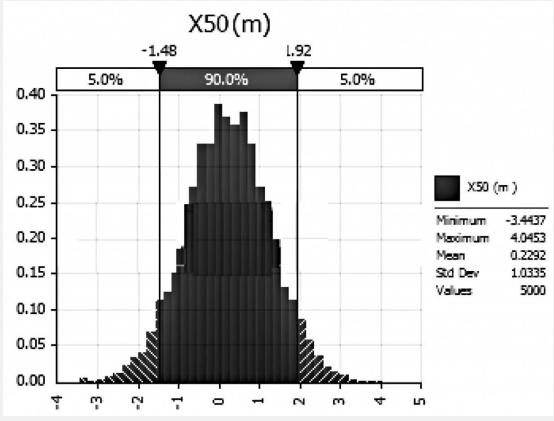

Figure 3. Probability density model for mean fragment size prediction.

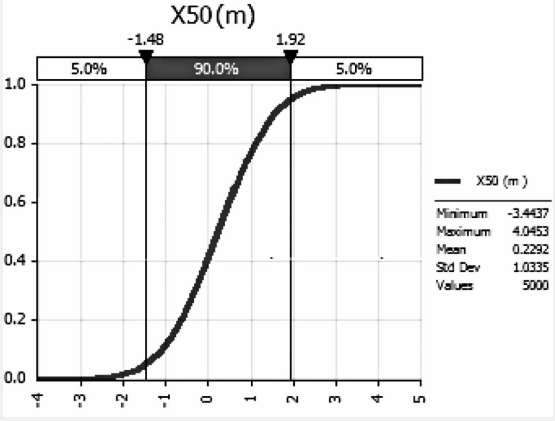

Figure 4. Cumulative probability density curve.

Table 6. Output result of the simulation.

Name	Graph	Min	Mean	Max	5%	95%
X50 (m)		-3.44373	0.2292396	4.04533	-1.482735	1.923781

3.2.1 Sensitivity analysis

Furthermore a sensitivity analysis is done with @risk and decision support tool. The important of this analysis is to show the influence of the parameters on fragmentation. This allows ranking the effects of the parameters or the predictors on mean fragmentation. The input probability distribution variables in Table 5 is model in such as way that the input varies within -10% to 10 % of their mean value, each variable at a time keeping the other constant and the output , mean fragmentation determined. This is simulated for five thousand times, with each value of the variable and outcome recorded. The variables are ranked with the output. The result shows that fracture toughness and brittleness are more important and ranked higher being more sensitive on fragmentation result than ratio of spacing to burden and powered factor (Figure 5). The detailed model statistic and percentage variation in the both the input and the outcome are shown in Table 7. Therefore fracture toughness and brittleness are more important and sensitive to the prediction of fragmentation. Fragmentation of course depends on these parameters as mechanical properties influencing fragmentation.

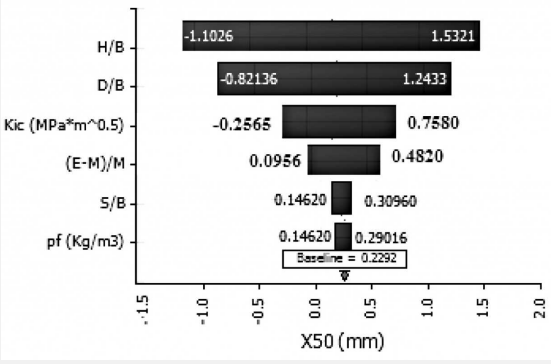

Figure 5. Sensitivity of parameters to mean fragments size prediction.

Table 7. Detailed statistic.

Description	X50 (mm)	Kic (MPa*m^0.5)	S/B	H/B	D/B	pf (Kg/m3)	(E-M)/M
Minimum	-3.44373	0.9642427	0.6850145	0.2789843	0.000579241	-0.6831121	-0.3234654
Maximum	4.04533	2.191194	1.340409	9.07725	0.005078671	1.46543	-0.02472234
Mean	0.2292396	1.619712	1.015115	4.494382	0.002770326	0.4450026	-0.1706185
Std Deviation	1.03354	0.1684087	0.09664208	1.219658	0.000607158	0.2601825	0.04077379
Variance	1.068206	0.0283615	0.00933969	1.487565	3.68641E-07	0.06769492	0.001662502
Skewness	-0.0199564	-0.02438528	0.007344594	-0.03864793	0.01084502	-0.04762005	0.007904449
Kurtosis	2.932035	2.915846	2.880643	2.977987	2.977668	3.055586	2.951378
Mode	0.458768	1.555597	0.9882979	4.893261	0.002589207	0.4838571	-0.1671076
5% Perc	-1.482735	1.341823	0.8556129	2.492469	0.001777817	0.01856153	-0.2370981
10% Pere	-1.09791	1.403043	0.8935878	2.93296	0.001991378	0.1053071	-0.2232426
15% Pere	-0.8351	1.445181	0.916278	3.231998	0.002141534	0.1722599	-0.2136873
20% Pere	-0.6322749	1.477131	0.9334671	3.465132	0.002261152	0.2282353	-0.2060211
25% Pere	-0.4686274	1.506287	0.94791	3.658492	0.002354105	0.267312	-0.1980958
30% Pere	-0.325326	1.530354	0.9630346	3.846378	0.002449586	0.3062161	-0.191961
35% Pere	-0.1756062	1.553959	0.9760299	4.02343	0.002529834	0.3481895	-0.1860093
40% Pere	-0.03730343	1.576272	0.9893272	4.195568	0.002615048	0.3787448	-0.1807125
45% Pere	0.0879121	1.597468	1.001154	4.346839	0.002689132	0.4121803	-0.1756348
50% Pere	0.2240776	1.620875	1.013527	4.509325	0.002763721	0.44666	-0.1702
55% Pere	0.3638707	1.641825	1.026183	4.652012	0.002844113	0.4810571	-0.1657324
60% Pere	0.5043754	1.664858	1.03872	4.808883	0.002925806	0.5145342	-0.1605643
65% Pere	0.6443464	1.687125	1.051666	4.975644	0.003006358	0.5483432	-0.1550074
70% Pere	0.7711118	1.709155	1.067079	5.144704	0.00309085	0.5830716	-0.1495595
75% Pere	0.9310366	1.734253	1.081785	5.327464	0.003181219	0.6220999	-0.1430252
80% Pere	1.114335	1.762117	1.098858	5.52627	0.003271453	0.666389	-0.136325
85% Pere	1.317241	1.7954	1.117409	5.761966	0.003398983	0.7186224	-0.1283101
90% Pere	1.531171	1.836953	1.140501	6.05502	0.003544644	0.774826	-0.1177809
95% Pere	1.923781	1.89708	1.178248	6.502771	0.003774332	0.8631175	-0.1036816

4. CONCLUSIONS

Fracture toughness and brittleness of rock related to fragmentation and they can be use to predict it. It is shown that both parameters influence the degree of fragmentation than the powered factor and spacing to burden ratio. Since fragmentation response to dynamic load of Class I and Class II rocks differs it is reasonable to provide equation separately for them. A further research is to develop an equation for Class I quarry outcrops which are common with carbonates rocks like calcite, limestone, marble, gypsums and dolomites etc. The outcrops used in this work are granitic and similar outcrop that are Class II rocks are quartzite.

REFERENCES

Cunningham, C.V.B. 1983. The Kuz–Ram model for prediction of fragmentation from blasting. In: *First international symposium on rock fragmentation by blasting. Lulea, Sweden,* Lulea University Technology, p. 439–53.

Gheibie, S. Aghababaei, H. Hoseinie, S.H. Pourrahimian, Y. 2009. Modified Kuz–Ram fragmentation model and its use at the Sungun Copper Mine. *International Journal of Rock Mechanics and Mining Sciences;* 46(6):967–973.

Hall, J. & Brunton, I. 2002. Critical comparison of Kruttschnitt Mineral Research Center (JKMRC) blast fragmentation models. *Fragblast*; 6(2):207–220.

Hjelmberg, H. 1983. Some ideas on how to improve calculations of the fragment size distribution in bench blasting. In: *First international symposium on rock fragmentation by blasting. Lulea* Sweden, Lulea University Technology, p. 469–94.

Hudaverdi, T. Kulatilake, P. H. S. W. & Kuzu, C. 2010. Prediction of blast fragmentation using multivariate analysis procedures. *Int. J. Numer. Anal. Meth. Geomech,* Wiley Online Library, DOI: 10.1002/nag.957.

International Society for Rock Mechanics Commission on Testing Methods. (2007). In Ulusay R., Hudson J. A. (Eds.), *The pre failure and post failure ISRM suggested methods for rock characterization, testing and monitoring: 1974-2006. Ankara, Turkey: Commission on Testing Methods,* International Society of Rock Mechanics, Pergamon Press Ltd.

Kuznetsov, V.M. 1973. The mean diameter of the fragments formed by blasting rock. *Soviet Mining Science* 9(2):144–8.

Latham, J.P. Kemeny, J. Maerz, N. Noy, M. Schleifer, J. & Tose, S.A. 2003. Blind comparison between results of four image analysis systems using a photo-library of piles of sieved fragments. *Fragblast* 7(2):105–132.

Monjez, M. Rezaei, M. Yazdian Varjani, A. 2009. Prediction of rock fragmentation due to blasting in Gol-E-Gohar iron mine using fuzzy logic. *International Journal of Rock Mechanics & Mining Sciences* 46, 1273–1280.

Sanchidrian, J.A. Segarra, P. Lopez, L.M. 2007. Energy components in rock blasting. *International Journal of Rock Mechanics and Mining Sciences;* 44(1):130–147.

Tarasov, B. & Potvin, Y. 2013. Universal criteria for rock brittleness estimation under triaxial compression. *International Journal of Rock Mechanics & Mining Sciences* 59, 57–69.

Wawersik, W. R. & Fairhurst, C. 1970. A study of brittle rock fracture in laboratory compression experiments. *International Journal of Rock Mechanics and Mining Sciences & Geomechanics Abstracts,* 7(5) 561-564, IN7-IN14, 565-575.

Whittaker, B.N. Singh, R.N. & Sun, G. 1992. Rock fracture mechanics: principles, design and applications. Elsevier, Amsterdam.